

19941228 003

MODEL OF A SINGLE IMPURITY IN A WIDE
BANDGAP SEMICONDUCTOR DESCRIBING
ELECTRIC FIELD SCREENING

THESIS

Anthony N. Dills, Second Lieutenant, USAF

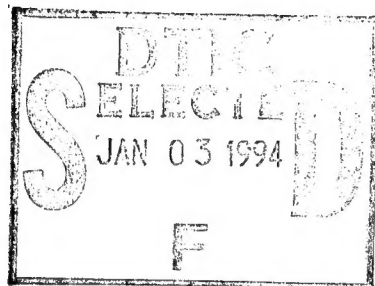
AFIT/GAP/ENP/94D-3

This document has been approved
for public release and sale; no
distribution is unlimited.

DEPARTMENT OF THE AIR FORCE
AIR UNIVERSITY
AIR FORCE INSTITUTE OF TECHNOLOGY

Wright-Patterson Air Force Base, Ohio

AFIT/GAP/ENP/94D-3



Accession For	
NTIS CR/CI	<input checked="" type="checkbox"/>
DTIC TAB	<input type="checkbox"/>
Unannounced	<input type="checkbox"/>
Justification	
By	
Distribution /	
Availability Codes	
Dist	Avail. and/or Special
A-1	

**MODEL OF A SINGLE IMPURITY IN A WIDE
BANDGAP SEMICONDUCTOR DESCRIBING
ELECTRIC FIELD SCREENING**

THESIS

Anthony N. Dills, Second Lieutenant, USAF

AFIT/GAP/ENP/94D-3

DTIC QUALITY INSPECTED 2

Approved for Public Release; Distribution Unlimited

The views expressed in this thesis are those of the author and do not reflect the official policy or position of the Department of Defense or the U. S. Government.

AFIT/GAP/ENP/94D-3

MODEL OF A SINGLE IMPURITY IN A WIDE BANDGAP SEMICONDUCTOR
DESCRIBING ELECTRIC FIELD SCREENING

THESIS

Presented to the Faculty of the Department of Physics

of the Air Force Institute of Technology

In Partial Fulfillment of the

Requirements for the Degree of

Master of Science in Applied Physics

Anthony N. Dills, B.S.

Second Lieutenant, USAF

December 1994

Approved for public release; distribution unlimited

Preface

This research is an investigation to determine if and under what conditions general analytical solutions for electric field screening could be applied to wide bandgap semiconductors such as bismuth silicate. The analytical solutions are based upon a single impurity level within a wide bandgap semiconductor. If screening for bismuth silicate could be described using a single impurity level, then this would greatly simplify the numerical calculation involved in a two dimensional model currently being investigated by Major Gary D. Barmore. I found this work to be gratifying because I learned a great deal more about semiconductors and the dynamics within them. Prior to this effort, my mind was full of bits and pieces of physics acquired from classes. Now I understand how several of the pieces fit together, and I am eager to add more pieces in the future.

I would like to thank my advisor, Dr. T. E. Luke, for opening a new door of semiconductor physics to me. His support, encouragement, and forever open door policy was greatly appreciated. Also, Major Gary D. Barmore, who is soon to receive his Ph.D. in physics, was very instrumental in initially getting me “up to par” and in bridging the gap between instructor and student terminology. I thank my wife for her continued support through this effort. She would always know when I needed room and when I needed encouragement. Thank you my son, Caleb, who always knew how to make Daddy smile. Most of important, my thanks goes to my Lord and Savior, Jesus Christ, who gave me the patience and persistence to complete this thesis.

Anthony N. Dills

Table of Contents

	Page
Preface _____	ii
List of Figures _____	v
List of Tables _____	vii
List of Roman Symbols _____	viii
List of Greek Symbols _____	ix
Abstract _____	x
I. Introduction _____	1
II. Background _____	5
General _____	5
Screening _____	7
III. A. S. Furman's paper _____	10
Screening and Stratification _____	10
Description of Cases _____	13
Case One: Shallow Donors, $\tau_i \ll \tau$ _____	15
Case Two: Deep Donors, $\tau \ll \tau_i \ll \tau_M$ _____	15
Case Three: Deep Donors, $\tau \ll \tau_M \ll \tau_i$ _____	16
The rate equations _____	16
The solutions and their assumptions _____	20
Case One: Shallow Donors, $\tau_i \ll \tau$ _____	20
Case Two: Deep Donors, $\tau \ll \tau_i \ll \tau_M$ _____	21
Case Three: Deep Donors, $\tau \ll \tau_M \ll \tau_i$ _____	22
IV. Single Donor Level _____	26
Numerical simulation _____	26
Normalization _____	30
Results _____	32
Constant Electron Lifetime Results _____	34
Explicit Examination of Constant Electron Lifetime Assumption _____	39
V. Single Trap Level _____	45
Numerical simulation _____	45
Results _____	50

	Page
VI. Conclusions and Recommendations _____	52
Appendix A: The PRIZ Device _____	54
Appendix B: Derivation of Fermi Energy Level _____	58
Appendix C: Derivation of β/γ for the Single Donor Level Model _____	60
References _____	61
Vita _____	63

List of Figures

Figure	Page
1. A typical model of a wide bandgap semiconductor. This is one of the models used for bismuth silicon oxide (BSO). The energy band gap is 3.25eV while the donor and traps are labeled respectively. _____	2
2. The modeled crystal defined by a length d with an applied voltage V . The direction of the electric field is in the negative direction. _____	6
3. A qualitative picture explaining the initial neutral charge throughout the crystal. _____	7
4. Band diagram showing the ionized donor sites and the free electrons under the influence of the applied electric field. The darkened oval depicts the formation of the net positive region as the free electrons drift toward the anode. The black dots are the free electrons and the hollow dots with the plus (+) signs are the ionized donor sites. CB = conduction band. VB = valence band. _____	8
5. Pictorial description of internal fields generated by net space charge movement. The wide the electric field represents a stronger field. _____	9
6. Qualitative description of the net space charge ρ , the free electron concentration n , and the magnitude of the electric field $ E $. (a) and (b) depict the first and second space charge layers while (c) and (d) depict the three space charge regions. ⁵ _____	12
7. Plot of Eq (8) for case two deep impurities. The electric field is normalized to the applied field magnitude, V/d . The crystal length is normalized to the crystal length, d . _____	22
8. Case three analytical solution for different time slices. Figure (a) is for times much less than the Maxwellian relaxation time. Figure (b) shows oscillatory behavior of the electric field can only occur outside the Maxwellian time. For times outside the Maxwellian time, the field equation is invalid. _____	24
9. Case 2 comparison of numerical calculations (a) and analytical calculations (b) of the electric field distribution taken at four specific time slices (see Table 4) and assuming the lifetime of the free electron is constant. _____	36

Figure	Page
10. Case 3 comparison of the numerical calculations (a) and the analytical calculations (b) of the electric field distribution taken at four specific time slices (see Table 4) and assuming the lifetime of the free electron is constant. The depletion layer thickness in both calculations increases in time and no oscillations occur prior to the Maxwellian time. The movement of the electric fields as well as the cathode field magnitudes are consistent between the numerical results and Furman's analytical results.	37
11. Extended times larger than the Maxwellian time for Case 3 are used here to compare the numerical calculations and Furman's analytical calculations of the electric field distribution. These plots assume the lifetime of the free electron is constant. The depletion layer size now switches direction and decreases in time. The oscillations that do occur are short lived. Figure (b) is presented here only to emphasize the inaccuracy of Furman's solutions in this time regime.	38
12. Numerical results depicting a non-constant lifetime of electrons for case three and for specific times slices prior to the transit time (see Table 4).	39
13. Numerical results depicting a non-constant lifetime of electrons for case three and for specific times slices after the transit time (see Table 4). At later times the system approaches equilibrium and steady state.	40
14. Numerical calculations of the electric field distribution for Case 2 with a non-constant electron lifetime. The electric field does not agree with that predicted by Furman.	41
15. Numerical calculations of the electric field distribution for Case 3 with a non-constant electron lifetime and for times within the transit time. The depletion layer thickness and magnitude increase in time as predicted analytically.	42
16. Numerical calculations of the electric field distribution for Case 3 with a non-constant electron lifetime and for times much larger than the transit time. The depletion layer thickness and magnitude increases in time as predicted analytically.	43
17. Band diagram showing the ionized trap sites and the free electrons under the influence of an applied voltage.	46
18. A picture to help explain the different concentrations of electrons involved in the trap model.	49
19. Trap level model of the electric field for Case 3 as a function of the crystal length. Oscillations occur at very long times and with very small amplitude changes.	51

List of Tables

Table	Page
1. Initial parameter set for the crystal. _____	29
2. Conversion to normalized parameters. The primed variables are unnormalized. _____	31
3. List of unnormalized and normalized parameter values as well as a description of each. _____	32
4. Comparison of the observation time slices as different ratios. _____	34
5. Trap level model parameters. _____	50

List of Roman Symbols

Parameter Symbol	Description of Parameter	Unit
d	crystal length	m
D	diffusion coefficient	m ² / sec
e	magnitude of the electron charge	coul
E	internal electric field	volt/cm
E _D	donor energy below conduction band	eV
E _F	Fermi energy level in E _{gap}	eV
E _{gap}	bandgap energy separation	eV
E ₀	applied electric field	eV
E _T	trap energy below conduction band	eV
h	Planck's constant	joules sec
H	magnetic field intensity	Wb
i(z,t)	total current density	amp/m ²
I	illumination intensity	watt/m ²
j(z,t)	free electron current density	amp/m ²
k _B	Boltzmann's constant	joule/K
l ₀	drift length	m
m _e	mass of an electron	kg
m _{eff}	effective mass of the crystal	kg
n	free electron concentration	cm ⁻³
n _{norm}	density normalization factor	cm ⁻³
n ₀	number density of free electrons	cm ⁻³
n _p	number density of electrons photogenerated	cm ⁻³
n _T	number density of trapped electrons	cm ⁻³
n _{T0}	initial number density of trapped electrons	cm ⁻³
N _C	effective density of states in the conduction band	cm ⁻³
N _D	donor concentration	cm ⁻³
N _D ⁺	ionized donor concentration	cm ⁻³
S	photoionization cross section	m ²
t	time	sec
t ₀ or t ₀	transit time	sec
T	temperature	K
V	applied voltage	volt
W	steady state depletion layer thickness	m
z	distance from cathode	m
z ₀	depletion layer thickness	m

List of Greek Symbols

Parameter Symbol	Description of Parameter	Unit
β	ionization rate	sec^{-1}
ϵ	permittivity	Farad/cm
γ	recombination coefficient	$\text{cm}^3 \text{sec}^{-1}$
μ	mobility of free electrons	$\text{cm}^2 / \text{V sec}$
ρ	net charge density	$\text{coul} / \text{cm}^{-3}$
τ	free electron lifetime	sec
τ_i	ionization time	sec
τ_M	Maxwellian relaxation time	sec

Abstract

A mathematical model of the influence on electric field screening arising from a single impurity in a wide bandgap semiconductor has been numerically investigated and compared with analytically derived solutions. The parameter set chosen to perform the comparison of analytical solution and numerical solution is based upon a bismuth silicate crystal. Both the analytical calculations and the numerical calculations are an attempt to mathematically model the internal electric field within a semiconductor. Two types of impurities were looked at: a single donor level and a single trap impurity level. In general, after an abrupt application of a voltage across the semiconductor, net charge regions begin to redistribute and create internal electric fields that screen the applied field. A trap impurity is found to be more self-consistent with the analytical solutions than a donor impurity; the former satisfying the assumption of a constant free electron lifetime. The analytical solutions are valid for observation times much less than the Maxwellian relaxation time τ_M : $t \ll \tau_M$. The analytical solution properly predicts stratification conditions when the observation time is prior to τ_M ; however, oscillatory behavior, characteristic of stratification, of the internal electric field occurs for times much greater than τ_M . During this regime the analytical solutions are invalid.

MODEL OF A SINGLE IMPURITY IN A WIDE BANDGAP SEMICONDUCTOR DESCRIBING ELECTRIC FIELD SCREENING

I. Introduction

Electric field screening is a typical response in a wide bandgap semiconductor that has been subjected to an external electric field in which injection is not sufficient to maintain charge neutrality. Screening refers to an internal modification of the external electric field. In effect, the changing internal field creates internal forces on the mobile carriers. These forces differ from the external force created by the external electric field. From the change in forces, the mobile carriers are screened from the external field.

Different mathematical models exist to describe screening. These models can be very complicated in that many species are involved. As shown in Figure 1 some models like that of bismuth silicate use a deep donor site and one or more trap sites. The mathematics describing the charge dynamics can quickly become very cumbersome with these complex models. In fact, closed form solutions are usually impossible to derive. For this reason, these mathematical models with many impurity sites can only be solved numerically. Recent work by A.S. Furman claims that screening in most wide bandgap semiconductors held at thermal equilibrium can be accurately modeled with one impurity level which is the source of thermally generated electrons. Using only a single impurity, Furman derives a closed form solution for the internal electric field which screens the external electric field. A closed form solution has

many advantages. The obvious being a great reduction in numerical calculations, while another advantage is a closed form solution facilitates the validation of experimental results.

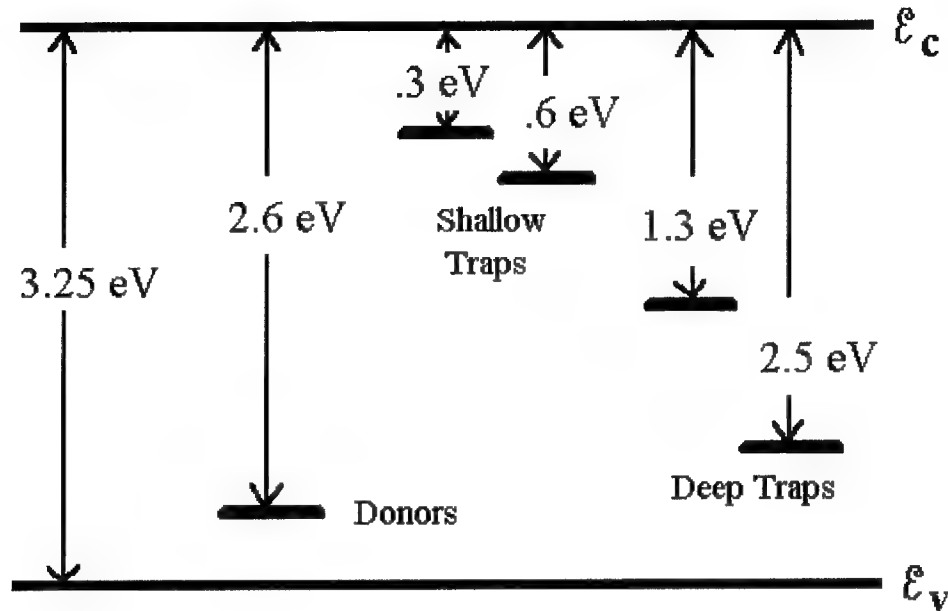


Figure 1. A typical model of a wide bandgap semiconductor. This is one of the models used for bismuth silicon oxide (BSO). The energy band gap is 3.25eV while the donor and traps are labeled respectively.

The purpose of this thesis is to numerically determine if, and under, what conditions A.S. Furman's analytical solution can accurately describe the dynamics of field screening. This task will be accomplished by numerically validating or disproving his solutions. To realistically accomplish this task, both the analytical solutions derived by Furman and the numerical solutions must be based on a real example. In his example, Furman alludes to a bismuth silicate (bismuth silicon oxide, BSO) crystal with an applied electric field in which injection is not sufficient to maintain charge neutrality. Typically, BSO is characterized by a deep donor level and many trap levels similar to those shown in Figure 1.^{1,2} A deep donor is donor site whose energy level is located far from the conduction band. Previous work with

BSO yields good agreement with experimental results when BSO is modeled with one deep impurity level and one or more shallow trap levels.² Even so, no analytic solution exists. If a single impurity level model with an analytic solution can accurately describe the screening dynamics involved in BSO, then theoretical comparisons to experimental observations of screening can become easier and exact with an analytical solution. For this reason, this thesis uses a parameter set that should reflect screening within BSO modeled with a single impurity level. This analysis is very similar to the analysis of a PRIZ device of which BSO is the active medium placed between transparent electrodes. Appendix A has more information concerning the PRIZ.

To obtain a goal one must set some milestones to accomplish along the way. The first milestone is to understand Furman's model of a single impurity level. This includes an analysis of the physics behind the different processes as well as the assumptions used to derive Furman's analytical solutions. The second milestone is to analytically derive estimates for some of the parameters needed to calculate the numerical solutions and to evaluate Furman's analytical solutions. These parameters include lifetimes and rate coefficients. The third milestone is to validate Furman's analytical solutions by using numerical routines available in MatLAB[®] to solve the rate equations describing the time and spatial evolution of the internal electric field. Once obtained, the numerical solutions will be compared to Furman's analytic solutions to determine when Furman's analytical solutions accurately describe the dynamics of electric field screening.

This chapter serves as an introduction to the problem, and the background in Chapter II defines the experimental setup for the single impurity model as well as many of the terms and processes involved. The third chapter is a full description of the contents of A.S.

Furman's paper to include the mathematical model described by a set of rate equations and their solution. Chapters IV and V explain numerical solutions to the same rate equations applied to the single donor level model and to the single trap level model that explains some of the discrepancies the numerical solution gave when compared to the analytical solution. Chapter VI concludes the thesis with a summery of results, conclusions, and recommendations. Appendix A gives an explanation of the PRIZ device and the BSO crystal.

II. Background

General

This research uses an experimental setup shown in Figure 2 that is common among all the models of wide bandgap semiconductors. Initially the system is assumed to be under thermal equilibrium. At time equal to zero an external field is applied from a contact on each end of the crystal where the injection of electrons is prohibited by a non-injecting cathode. The applied electric field is negative because the field points toward the cathode and the coordinate system begins at the cathode for $z = 0$ and ends at the anode for $z = d$. Because the focus is on extrinsic wide bandgap semiconductors, impurities exist. The types of impurities and their concentrations vary depending on the crystal.

The two types of impurity energy levels investigated in this research are a donor level and a trap level. For an electron carrier, a donor site is a neutral species within a crystal that has a high probability of contributing an electron to the conduction band when subjected to an excitation mechanism. Once the donor loses an electron, the donor becomes positively ionized. The current research focuses on thermal excitation, which in thermal equilibrium is governed by Fermi statistics. A trap site is a neutral species within a crystal that can capture an electron from the conduction band. Similar to the donor, once the trap gains an electron, the trap is negatively ionized. This site is different from a conventional recombination center in that the trapped electron has a higher probability of returning to the conduction band rather than recombining with ionized donors or holes in the valance band. To get a feel for relative impurity levels, in BSO shallow electron traps are normally 0.2 eV to 0.8 eV from the

conduction band, and the donor levels are around 2.6 eV from the conduction band. Typically, the donor levels are lie at any energy level depth within the energy bandgap. A conventional semiconductor donor is an impurity that replaces one of the semiconductor atoms, but the donor in BSO originates from a crystal defect.³

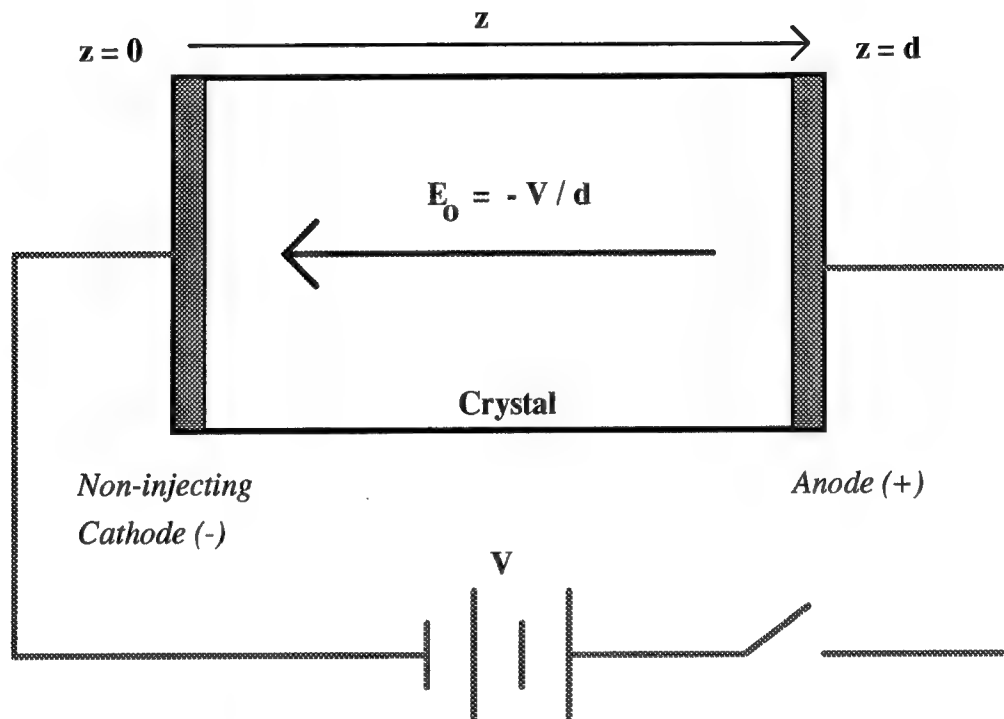


Figure 2. The modeled crystal defined by a length d with an applied voltage V . The direction of the electric field is in the negative direction.

The effect of both trap impurities and donor impurities are investigated in this research; however, they are treated separately in order to maintain a single impurity model. In the following qualitative discussion, the donor impurity is used to describe the physics behind field screening.

Screening

A simple one level donor impurity model will suffice to explain screening dynamics. As stated in the introduction, the system is held in thermal equilibrium. In thermal equilibrium, an initial concentration of electrons exists in the conduction band due to thermal excitation governed by Fermi statistics. These free electrons came from the donor level as shown in Figure 3.

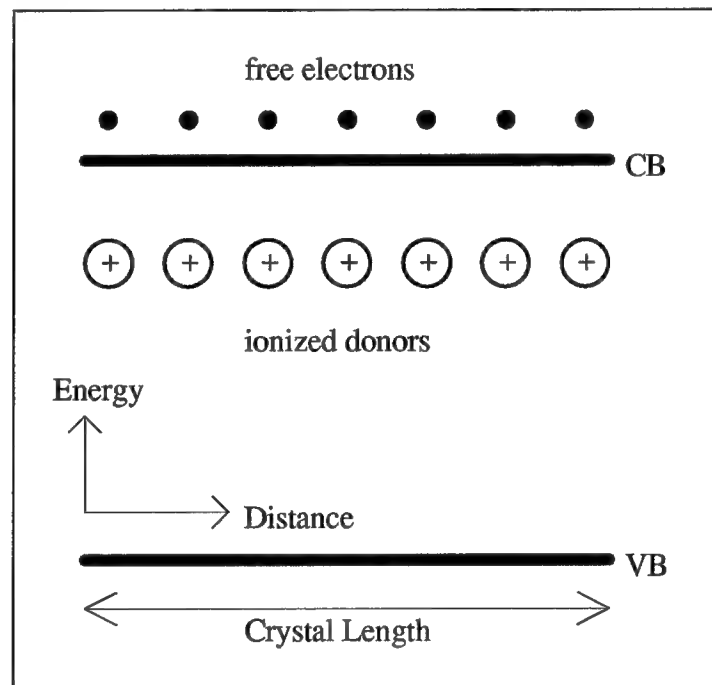


Figure 3. A qualitative picture explaining the initial neutral charge throughout the crystal.

Thus, the initial concentration of electrons is equal to the initial concentration of ionized donors. For this reason, before any electrical force is applied, the system has a net neutral charge throughout the crystal. Upon the application of an electric field, the free electrons move away from the cathode and toward the anode. Assuming a blocking contact at the cathode, the cathode region becomes positive since the ionized impurity level is a donor level

as seen in Figure 4 below. For future reference, the positive region near the cathode is called a depletion region.

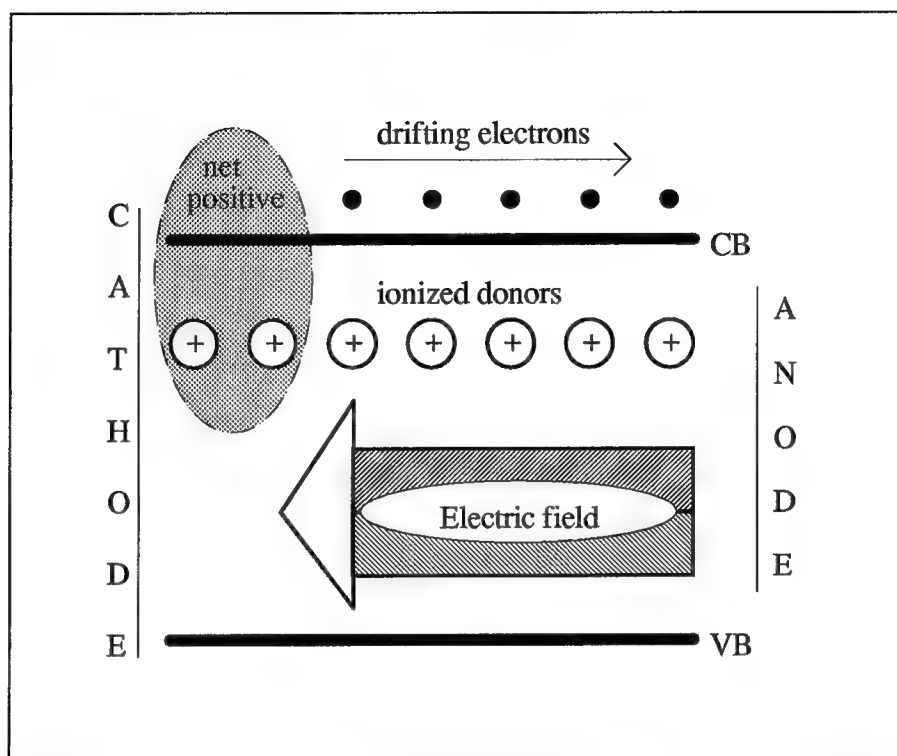


Figure 4. Band diagram showing the ionized donor sites and the free electrons under the influence of the applied electric field. The darkened oval depicts the formation of the net positive region as the free electrons drift toward the anode. The black dots are the free electrons and the hollow dots with the plus (+) signs are the ionized donor sites. CB = conduction band. VB = valence band.

As the charge distribution within the crystal changes under the influence of an external electric field, certain regions become more positive than others. For this reason, local fields are generated between different net space charge regions throughout the crystal. As a result, free electrons in a macroscopic region experience the influence of the external field modified by an internal field, which is spatially dependent. Some of the electrons may “feel” larger (or smaller) effects from the fields than others depending on their location within the crystal. For example, free electrons near the cathode may experience a stronger electric field force than do

the free electrons near the anode due to a large positive region forming near the cathode as shown in Figure 5. Between the cathode and the net positive region is a narrow regime where the electric field, potential divided by distance, is very large and pointing toward the cathode. This process of modulating the influence of the external field is referred to as screening. The following chapter discusses two types of screening.

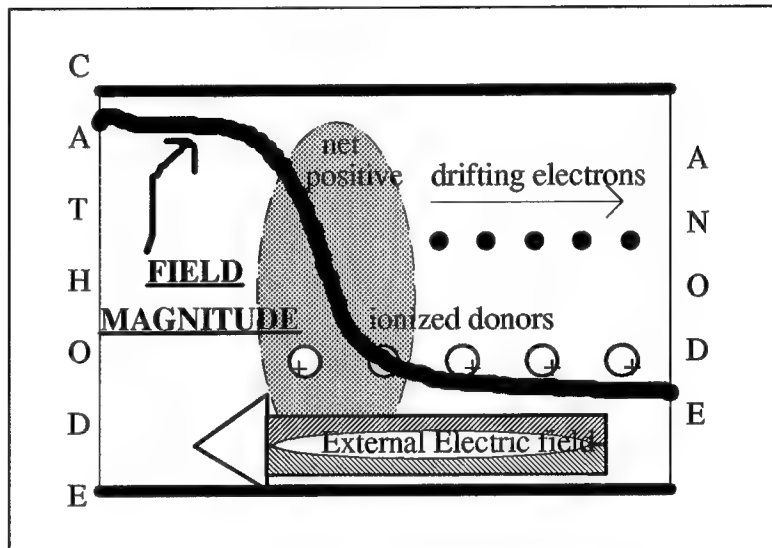


Figure 5. A sketch of internal fields generated by net space charge movement. The height the electric field represents a stronger field.

III. A. S. Furman's paper

Simple Screening

Chapter II introduced the concept of screening. Two types of screening exist, however. In one, the depletion region grows in thickness away from the cathode and in the other the net space charge regions redistribute to form alternating layers of net charge which create oscillations in the internal electric field. The first screening process does not have a specific name, while the second is called stratification.⁴ For simplicity in the rest of the paper, the term “simple screening” will refer to the first process.

As discussed in the previous chapter, all available free electrons leave the cathode region when the field is applied, thus the cathode region becomes positive. This net positive region is the depletion region. As time evolves, the free electrons continue to drift toward the anode. This movement causes the depletion region to increase its net positive charge and to expand in thickness away from the cathode until a steady state is reached. Steady state occurs when the free electron distribution becomes temporally constant.

The terms “steady state” and “equilibrium” are often confusing and misinterpreted. For this reason, a clear understanding of these terms is imperative before they are used in the following discussion. If a system has no external forces affecting it and if the internal particles, e.g., electrons, are perturbed slightly, then the particles will naturally relax back to equilibrium. The characteristic time for the particles to relax back to equilibrium is the Maxwellian dielectric relaxation time, τ_M , which is defined as the permittivity divided by the conductivity. Using this concept of equilibrium, steady state can be redefined as equilibrium

when a force is applied to the system. In the following analysis, the initial Maxwellian relaxation time is used as a measuring stick for when the system reaches steady state. Even though this characteristic time is for equilibrium, it still gives a good feel for the steady state time.

Stratification

Stratification is similar to simple screening; however, the space charge oscillates in the spatial dimension instead of monotonic change as in the simple screening. With stratification, the cathode depletion region thickness moves toward the cathode until reaching steady state, and the net space charge regions that develop have alternating net charges. This layering of space charge regions with alternating net charges is the stratification effect.⁴ Since Poisson's equation relates the electric field and the net space charge, oscillations occur in the electric field distribution as well. V.N. Astratov gives an excellent description of stratification and the parallel between space charge oscillations and electric field oscillations in his 1984 paper on "Stratification of the space charge in the case of screening of a field in crystals."⁵ Figure 6 delineates the basic process, which is discussed below.

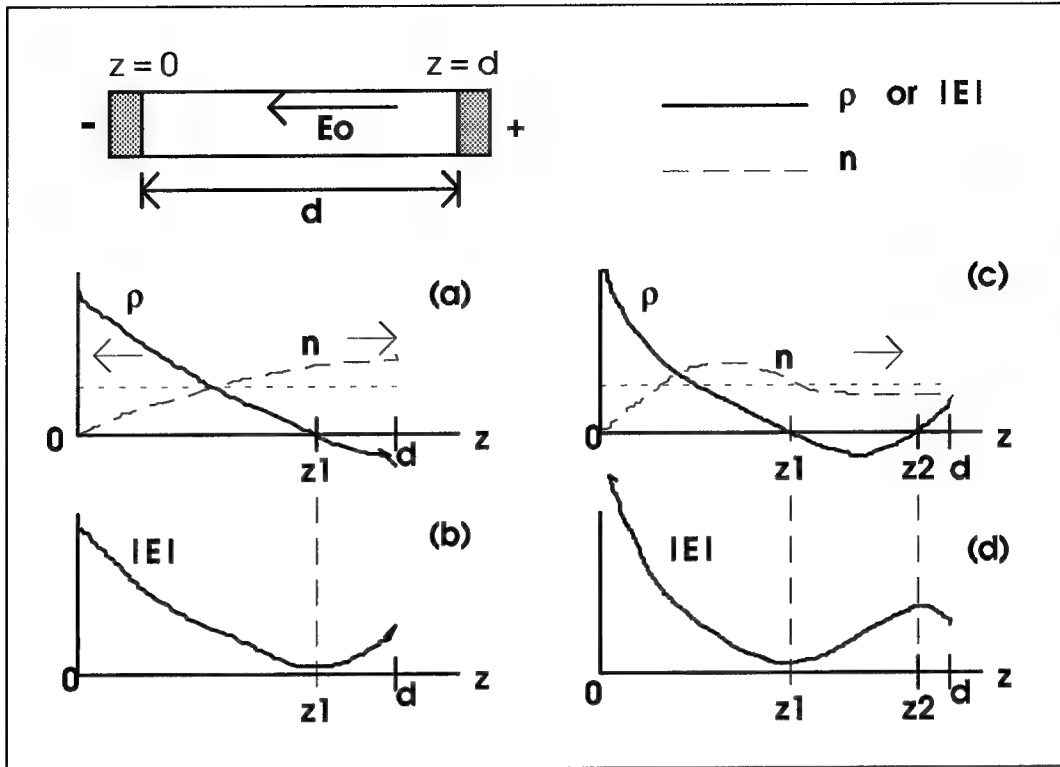


Figure 6. Qualitative description of the net space charge ρ , the free electron concentration n , and the magnitude of the electric field $|E|$. (a) and (b) depict the first and second space charge layers while (c) and (d) depict the three space charge regions.⁵

Before the application of the external field, an equilibrium exists between the generation of electrons to the conduction band and the recombination of electrons to the impurity level. During this initial time, the concentration of free electrons and the concentration of ionized impurities are in equilibrium and are uniformly distributed throughout the crystal. Thus the net charge density is zero over the entire crystal. Applying the field creates a force on the electrons and the positive ions. Assuming the ions remain stationary, only the electrons will drift toward the anode. Assuming no injection at the cathode, the movement of the electrons creates a region near the cathode, a depletion layer, that has a deficiency of electrons and therefore has a net positive charge. The formation of the positive

region near the cathode is the first layer of the space charge stratification, and the formation of the negative region near the anode is the second layer of the space charge region. According to Poisson's equation, $\nabla \cdot \mathbf{E} = \rho / \epsilon_0$, the point z_1 at which the space charge goes from positive to negative is the first local minimum of the electric field. As depicted in Figure 6, this inflection point is a minimum in the electric field, thus, it minimizes the amount of the force, qE , acting on the electrons and acts to prevent electrons from drifting past z_1 . This has two consequences. First, the electron concentration near z_1 will begin to increase and thus eventually creating a maximum in the electron distribution and a net reduced positive charge region just short of z_1 . This build up of the electron concentration continues until the net space charge just short of z_1 becomes negative. By becoming negative, the inflection point of the electric field has shifted to the left of z_1 . In effect, the depletion layer thickness has decreased or z_1 has moved to the left. Second, the decrease of electrons passing z_1 as well as the continued drift of electrons to the right of z_1 toward the anode creates another depletion region at z_2 where the net charge density is positive and the identical process discussed for z_1 will again happen at a new location z_2 where $z_1 < z_2$. This second process creates a third stratification layer and the process continues for more layers as the original depletion layer gets closer to the cathode.

Description of Cases

A. S. Furman's mathematical model⁶ addresses the dynamics of electric field screening to include stratification. His mathematical model serves as a good quantitative introduction into the problem. This model contains one impurity level and assumes a constant ionization rate and a constant lifetime of electrons in the conduction band. The boundary conditions

include a doped, n-type semiconductor with a static applied voltage and a potential barrier created by the metal contact and the semiconductor prohibiting the flow of electrons from crossing the cathode (no injection). Furman's model for one impurity level covers three cases with different characteristic times. The three cases are shallow impurities and two types of deep impurities.

The characteristic times that define the three cases are the ionization time τ_i , the free electron lifetime τ , the Maxwellian relaxation time τ_M , and the transit time t_0 . The ionization time is the inverse of the ionization rate, which characterizes how many electrons per second are thermally excited into the conduction band. The free electron lifetime is the average time the free electron is in the conduction band. As discussed earlier, the Maxwellian relaxation time is the time in which the system of free electrons and ions reach equilibrium. If the initial concentration of free electrons is known, then the Maxwellian time in seconds is defined as

$$\tau_M = \frac{\epsilon}{\sigma} = \frac{\epsilon}{e \mu n_0} \quad (1)$$

where ϵ is the semiconductor permittivity, e is the electron charge, μ is the electron mobility, and n_0 is the initial concentration of electrons in the conduction band. This Maxwellian time is, in general, dependent on the changing electron concentration; however, using the initial concentration of electrons allows the use this time as a characteristic time of the system. Its use is primarily to help distinguish between the three cases of screening. The fourth characteristic time is the transit time. The transit time is the initial time for an electron to drift across the semiconductor and is defined as the crystal length divided by the electron drift velocity. The electron drift velocity can be written as the drift mobility times initial internal field which equals the external electric field. The external electric field is in turn defined as the

applied potential voltage divided by the crystal length. Thus, in terms of the device parameters, the transit time can be written as $d^2 / (\mu V)$ where d is the crystal length, μ is the free electron drift mobility, and V is the applied voltage across the crystal.

Case One: Shallow Donors, $\tau_i \ll \tau$. In case one, shallow donors lead to a very short ionization time τ_i when compared to the electron lifetime τ , i.e. $\tau_i \ll \tau$. Since the ionization time is very short or the ionization rate is very large, all the available electrons are excited into the conduction band and convectively transported from the cathode region before recombination of free electrons occur in τ . As explained in Chapter I, the depletion layer thickness grows in time.

Case Two: Deep Donors, $\tau \ll \tau_i \ll \tau_M$. In case two, the donor level is further away from the conduction band, thus the donor is called a deep donor. The term “deep” is not the typical deep donor in semiconductor that is 2 eV or more below the conduction band. Instead, the donor in this case, and in the latter case, is on the order of 0.8 eV which is considered deep when compared to 0.2 eV shallow donors. In this case, the free electrons have a lifetime less than the ionization time, but both of these times are much less than the Maxwellian relaxation time, $\tau \ll \tau_i \ll \tau_M$. With these characteristic times, the electrons recombine at a higher rate than they are generated and long before they can redistribute themselves to counter the internal electric fields. Under these conditions, recombination to the donor level will dominate, and in regions where this happens the net charge becomes less negative due to the loss of free electrons. Before equilibrium is established (prior to the Maxwellian time, $t \leq \tau_M$), more ionization occurs and the excited electrons recombine again. Thus the cathode region becomes more positive and the net positive space charge migrates

toward the anode as it does in Case 1. If the observation time is much greater than the Maxwellian time ($t \gg \tau_M$) then the recombination, generation, and charge redistribution reach equilibrium and the space charge distribution attains steady state.

Case Three: Deep Donors, $\tau \ll \tau_M \ll \tau_i$. For Case 3, the deep donor is similar to Case 2 but with the Maxwellian time between the other two characteristic times, $\tau \ll \tau_M \ll \tau_i$. With these characteristic times, the electrons recombine before they can redistribute and try to counter the internal electric fields. In addition, the electrons recombine long before they are thermally re-generated. Under an applied field, the initial electron density in the conduction band migrates to form a concentration of electrons in a region away from the cathode. The cathode region becomes more positive and the region containing the bulk of the electrons becomes more negative. Since the free electron lifetime is much shorter than the other characteristic times, a portion of the bulk electrons will recombine with the donor level. This results in a decrease in negative charge for this bulk region of free electrons. At this point the system has three distinct space charge regions like the ones in Figure 4, 5, and Figure 6. As a result of this net space charge behavior, stratification occurs. For this case, Furman says that for observation times much less than the ionization time, the ionization time and the lifetime of the free electrons are practically constant. With this observation, Furman solves the governing rate equations, which are described in the following discussion.

The rate equations

For each impurity energy level a rate equation exists as well as a rate equation for the free electrons. Furman explains his equation in terms of an unionized probability distribution function. For simplicity, the equations are rewritten in terms of ionized impurity

concentrations. The signs in Furman's rate equations suggest a donor impurity, thus the first of his two rate equations, Eq (2) and Eq (6), describes the rate of population change for the ionized donor concentration N_D^+ :

$$\frac{\partial N_D^+(z, t)}{\partial t} = \beta (N_D - N_D^+(z, t)) - \gamma \cdot N_D^+(z, t) \cdot n(z, t) \quad (2)$$

The first term on the right hand side is the generation term for ionized donors (or impurities), N_D^+ ; it depends on the number of unionized donors and a generation rate. The unionized donor concentration is the total minus the ionized donor concentration. Furman's generation term includes a summation of both a thermal generation coefficient β and a photogeneration term, $S \cdot I$, which is the product of the photoionization cross section and the illumination intensity. However, this thesis considers only the thermal generation. The second term on the right hand side of Eq (2) is a recombination term and consists of a thermal recapture coefficient γ , the number of ionized donors N_D^+ , and the free electron density n . This equation is often written in terms of characteristic times. Since this thesis compares characteristic times, rewriting Eq (2) is appropriate:

$$\frac{\partial N_D^+(z, t)}{\partial t} = \frac{(N_D - N_D^+(z, t))}{\tau_1} - \frac{n}{\tau} \quad (3)$$

where the ionization time τ_1 is $1/\beta$ and the recombination time τ is $1/[\gamma N_D^+(z,t)]$ which may or may not be a constant.

The second equation, which describes the rate of change in free electron density, is derived from the continuity equation. Furman's model consists of a single donor level between the conduction band and the valence band, thus the net charge density ρ is defined as

$$\rho(z, t) = e N_D^+(z, t) - e n(z, t) \quad (4)$$

and when put into the one dimensional continuity equation,

$$\frac{\partial j(z, t)}{\partial z} = - \frac{\partial \rho(z, t)}{\partial t} = -e \frac{\partial N_D^+(z, t)}{\partial t} + e \frac{\partial n(z, t)}{\partial t} \quad (5)$$

yields Furman's second rate equation:

$$\frac{\partial n(z, t)}{\partial t} = \frac{\partial N_D^+(z, t)}{\partial t} + \frac{1}{e} \frac{\partial j(z, t)}{\partial z} \quad (6)$$

where $j(z, t)$ is the free electron current density consisting of drift current $[e \mu n(z, t) E(z, t)]$ and diffusion current $[e D \partial n(z, t) / \partial z]$. Furman ignores the diffusion current when he solves these equations. Thus, when one compares the numerical results with Furman, one must solve the equations without diffusion current in the “ j ” term.

The third equation completing the set of governing equations is a relationship for the total electric field. In general, the total electric field is defined as the negative potential gradient, $E \equiv -\nabla \Phi$, and can be broken down into two parts, the external field plus the internal field. The external field is $-V/d$ and the internal field is defined by integrating Poisson's equation. At the cathode, the total electric field is the external field plus the internal field integrated over the entire crystal length,

$$E(0, t) = -\frac{V}{d} + \frac{1}{d} \int_0^d (z - d) \frac{\rho(z, t)}{\epsilon} dz$$

Elsewhere in the crystal, the total electric field is defined as the cathode electric field above plus the internal field integrated up to the current location, z , within the crystal. Thus the total electric field expression is

$$E(z, t) = E(0, t) + \int_0^z \frac{\rho(\xi, t)}{\epsilon} d\xi \quad (7)$$

where the system is held under a constant voltage, V , which is explicitly written as

$$V = - \int_0^d E(z) dz$$

and where the spatial dependence in the longitudinal direction and time dependence have been shown. For the true model of the semiconductor, the spatial dependence is three dimensional. These equations are the basic equations describing the dynamics of the screening of an electric field in a semiconductor with a donor level. They are spatially and temporally dependent, thus they are subject to initial and boundary conditions. The boundary conditions stated in Furman's paper use the fact that the total current density is a constant with respect to position. The total current density is the sum of the bound displacement current density, $\epsilon \partial E / \partial t$, and the free electron current density, $j(z,t)$. The second boundary condition assumes the applied voltage is held constant across the semiconductor. The first boundary condition comes directly from Maxwell's equation, $\nabla \times \mathbf{H} = \mathbf{j} + \frac{\partial \mathbf{D}}{\partial t} = \mathbf{i}$. Taking the divergence of each side yields zero for the change in total current as a function of a change in distance. Consistent with Furman's boundary conditions, one must assume that at the cathode ($z = 0$), no injection occurs. With this assumption, the free current density at the cathode is zero because no carriers exist in this region. The initial conditions also require the initial concentration of free electrons to be a set amount corresponding to the equilibrium temperature of the crystal. Under thermal equilibrium, this initial free electron concentration can be calculated from knowing basic semiconductor physics. (See Chapter IV, Eq (12).)

The solutions and their assumptions

Furman solves the two rate equations, Eq (3) and Eq (6), and then considers the three cases discussed earlier. The actual derivation of the solutions is not repeated in this research; however, the solutions and the assumptions governing them are discussed. In each of the three cases, Furman assumes the observation time is much less than the Maxwellian time. By assuming this, Furman can linearize the rate equations and combine them into one differential equation for each case.

Case One: Shallow Donors, $\tau_i \ll \tau$. In the first case of shallow impurities, a quasi steady state is established as a result of slow expansion of the depletion layer. Furman assumes the space charge is positive for locations within the depletion layer ($z \leq z_0$) and for $z > z_0$, the net space charge is zero because he assumes the electrons leave at the anode. In the following expression, z_0 tracks the depletion layer thickness and E shows the distribution of the electric field:

$$E(z, t) = \begin{cases} E_0 \left(1 - \frac{z_0(t)^2}{W^2} \right) - e n_0 (z_0(t) - z), & z \leq z_0(t) \\ E_0 \left(1 - \frac{z_0(t)^2}{W^2} \right) & , z \geq z_0(t) \end{cases} = W \tanh\left(\frac{t}{\tau_0}\right) \quad (8)$$

where n_0 is the initial concentration of carrier electrons; E_0 is the applied electric field defined as the applied voltage of $-V$ over the crystal length d ; W is the steady state thickness of the screened depletion layer defined as

$$W = \sqrt{\frac{\epsilon V}{e n_0}} = d \sqrt{\frac{\tau_M}{t_0}} \quad (9)$$

where ϵ is the permittivity of the semiconductor, e is the magnitude of the electron charge; and the characteristic time τ_0 is defined as

$$\tau_0 = \frac{1}{\mu} \left(\frac{2 \epsilon d}{e n_0 |E_0|} \right)^{1/2} = \sqrt{2 \tau_M t_0} \quad (10)$$

where μ is the mobility of the free electrons.

Case Two: Deep Impurities, $\tau \ll \tau_i \ll \tau_M$. For the first process of deep impurities, a local equilibrium is set up between electron generation and recombination. In this case, the change in ionized donors with respect to time, the first term in Eq (6), goes to zero and the rate equation for ionized donors, Eq (3), is ignored. The resulting rate equation describes the screening which is due to a redistribution of bound charge which can be treated, according to Furman, as a free electron gas characterized by a drift velocity. When the observation time, t , is much less than the Maxwellian time, τ_M , then the resulting linearized differential equation is the same as that derived for Case 1. For this reason, the Case 1 solution applies for Case 2. Because they have the same solutions, only Case 2 will be analyzed.

For Case 2, the plots of Eq (8) are given in Figure 7. This figure shows the depletion layer size increasing in time. Outside the depletion layer is a homogeneous electric field.

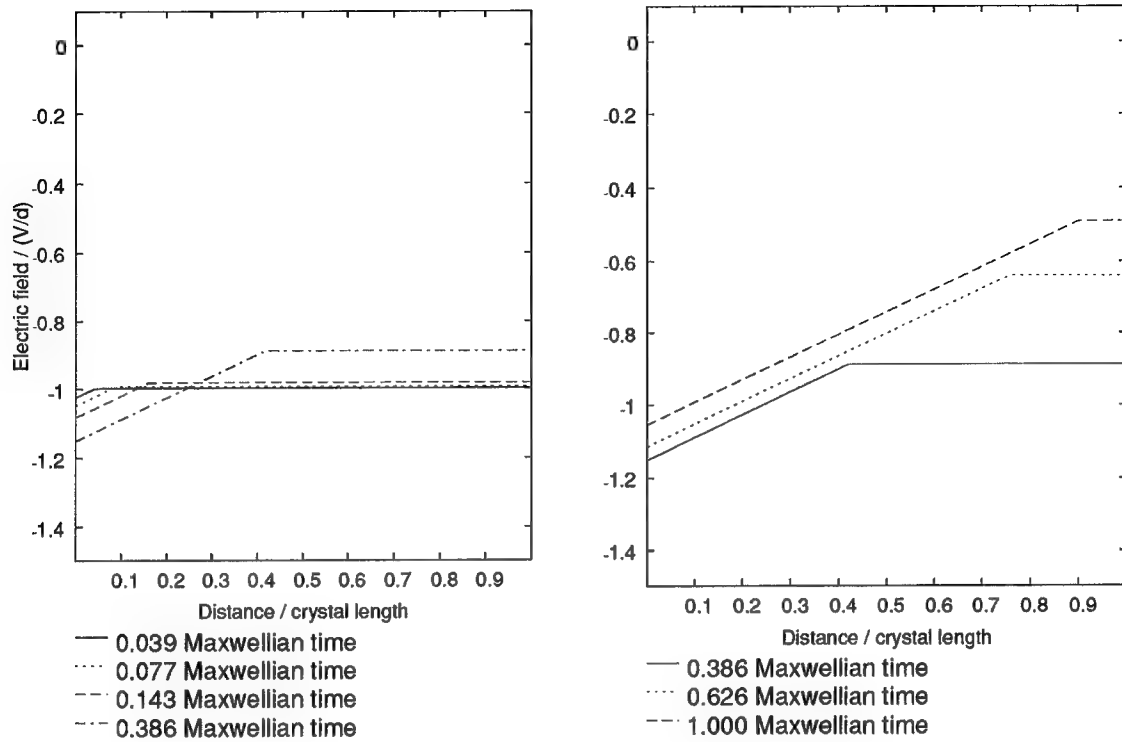


Figure 7. Plot of Eq (8) for case two deep impurities. The electric field is normalized to the applied field magnitude, V/d . The distance is normalized to the crystal length, d .

Case Three: Deep Impurities $\tau \ll \tau_M \ll \tau_i$. For the second case of the deep impurities,

Furman also achieves a solution. After approximating that the rate of generation and the electron lifetime remain nearly constant but not equal and that recombination dominates,

Furman derives this general solution:

$$E(z, t) = E_0 \begin{cases} 1 - A \cdot B \cdot C, & z \leq z_0 \\ 1, & z > z_0(t) = \frac{t}{\tau} l_0 \end{cases} \quad (11)$$

where

$$\begin{aligned}
A &= \left(\frac{t l_0}{\tau_M z} - \frac{\tau}{\tau_M} \right)^{1/2} \\
B &= \exp \left[- \frac{z}{l_0} \left(1 - \frac{\tau}{\tau_M} \right) \right] \\
C &= J_1 \left[2 \left(\frac{z}{l_0} \left(\frac{t}{\tau_M} - \frac{\tau}{\tau_M} \frac{z}{l_0} \right) \right)^{1/2} \right]
\end{aligned}$$

and where J_1 is the Bessel function of the first kind and l_0 is the drift length ($\mu \tau |E_0|$).

This equation has one primary restriction: $t \ll \tau_M$. Furman assumes $t \ll \tau_M$ in order to linearize and solve the differential equations that results in Eq (11). The plot of Eq (11) is shown in Figure 8. As in the previous two cases, simple screening occurs; however, stratification does not occur except for times outside the time restriction ($t > \tau_M$). Even though the field oscillations occur outside the Maxwellian time, Case 3 is the only case that stratification is observed analytically. The question is whether or not this stratification is real. Furman continues to say that the stratification can also occur for a third deep level case, $\tau_M \ll \tau \ll \tau_1$; however, according to Eq (11), it only occurs when $t > (\tau \tau_M)^{1/2} > \tau_M$ and Eq (11) is no longer valid.

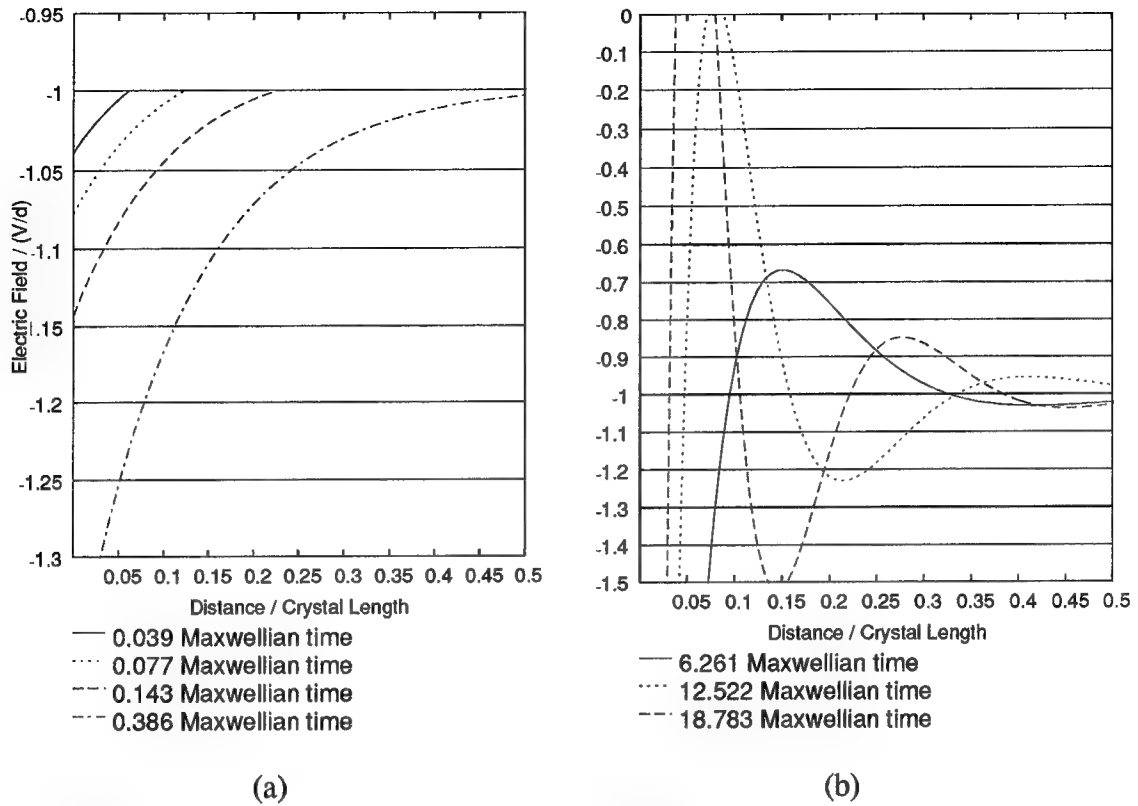


Figure 8. Case three analytical solution for different time slices. Figure (a) is for times much less than the Maxwellian relaxation time. Figure (b) shows oscillatory behavior of the electric field can only occur outside the Maxwellian time. For times outside the Maxwellian time, the field equation is invalid.

The plots in Figure 8 show two types of behavior as time increases. During $t < \tau_M$, the electric field distribution is nonlinear and approaches a normalized value of -1. Only for times greater than the Maxwellian time, $t > \tau_M$, does the electric field oscillate and exhibit stratification. The times in this region violate Furman's time restriction. For this reason, one may wonder why Furman reported oscillations. Even though his equations are invalid during this time regime, he still showed oscillatory behavior. This oscillatory behavior is not the same as that seen in the laboratory; however, he may have wanted to show that only oscillations exist. In order to accurately predict the single impurity level electric field

dynamics, one must solve the governing rate equations (Eqs (2) and (6)) numerically for all the times of interest.

The next two chapters numerically solve two examples of single impurity level models. Chapter IV contains an analysis of the single donor level, while the single trap level is analyzed in Chapter V. In both chapters, numerical results are compared to the previously obtained analytical results.

IV. Single Donor Level

Numerical simulation

Since thermal equilibrium conditions are assumed, a parameter set can be derived to properly model any single donor level in a wide-bandgap semiconductor. The following discussion analyzes the origin of a particular parameter set based upon thermal equilibrium conditions. The parameter set chosen coincides with bismuth silicate being the active medium. Bismuth silicon oxide (BSO) was chosen since Furman alluded to an example for which BSO was the active medium. By choosing a concrete example such as BSO, material properties such as mobility, permittivity, and donor energy level are known. The other parameters, such as characteristic times, must be calculated. These calculations are facilitated by thermal equilibrium conditions. The next few paragraphs explain how to determine a complete parameter set using thermal equilibrium conditions.

The basic parameter set includes three of the characteristic times discussed in the previous chapter. To reiterate, the three times are the ionization time τ_i , the free electron lifetime τ , and the initial Maxwellian relaxation time τ_M . Using first principles in physics, all of these times can be determined if the magnitude of one is arbitrarily chosen. In the following explanation, the lifetime of the free electrons is arbitrarily chosen to be 0.1 times the initial Maxwellian time. Thus the first characteristic time to calculate is the initial Maxwellian relaxation time. From Eq (1), the only unknown that must be calculated is the initial concentration of free electrons.

According to standard solid state texts,⁷ when a system is in thermal equilibrium, Boltzmann statistics accurately predict the thermal equilibrium concentration of electrons in the conduction band. For n-type semiconductors, this expression is written as:

$$n_0(T) = N_C(T) \exp\left(-\frac{E_{\text{gap}} - E_F(T)}{k_B T}\right) \quad (12)$$

where

$$N_C(T) = 2\left(\frac{2\pi m_{\text{eff}} k_B T}{h^2}\right)^{3/2} \quad (13)$$

is the effective density of states in the conduction band,⁸ E_{gap} is the bandgap energy separation which is assumed to be the conduction band energy level, k_B is Boltzmann's constant, T is the temperature in Kelvins, m_{eff} is the effective mass of the semiconductor, and h is Planck's constant. And as shown in Appendix B, solving the charge neutrality condition, $n_0 = N_d^+(t=0)$ for n-type semiconductors having only a donor level and for incomplete ionization, yields a Fermi level energy as

$$\begin{aligned} E_F(T) = & \frac{1}{2} (2E_{\text{gap}} - E_D) + \frac{k_B T}{2} \ln\left(\frac{N_D}{2 N_C(T)}\right) \\ & - k_B T \cdot \arcsin\left(\sqrt{\frac{N_C(T)}{8 N_D}} \exp\left(-\frac{E_D}{2 k_B T}\right)\right) \end{aligned} \quad (14)$$

where E_D is the donor energy level below the conduction band and N_D is the total donor concentration.

Once the equilibrium concentration of electrons is known, the Maxwellian relaxation time is easily calculated from the permittivity divided by the electrical conductivity:

$$\tau_M(T) = \frac{\epsilon}{\sigma} = \frac{\epsilon}{e \mu n_0(T)} \quad (15)$$

where ϵ is the permittivity, e is the elementary charge, μ is the electron mobility, and $n_0(T)$ is the initial electron concentration in the conduction band defined by Eq (12).

After calculating the Maxwellian time, the electron lifetime is known from the above choice for the ratio of τ_M to the electron lifetime τ . To reiterate, this choice for the ratio, τ / τ_M , is 0.1. This ratio says the Maxwellian time is much larger than the free electron lifetime and assumes the carrier electrons will not reach equilibrium during an observation time of $t < \tau_M$. With this assumption the lifetime of the free electrons is simply $\tau(T) = 0.1 \tau_M(T)$, which allows the determination of other parameters such as the drift length, $l_0(T) = \mu \tau(T) |E_0|$ and (from the second term on the right hand side of Eq (2)) the initial recombination coefficient:

$$\gamma(T) = \frac{1}{\tau(T) N_D^+(z, t = 0)} \quad (16)$$

where $N_D^+(z, t = 0)$ is the initial ionized donor concentration, which is equal to n_0 as long as the model consists of a single donor level with no injection occurring and no excitation from the valence band.

The relationship between the recombination coefficient and the ionization rate, $\beta = 1/\tau_i$, from solving Eq (2) under steady state conditions as shown in Appendix C is:

$$\beta(T) = \frac{\gamma(T)}{2} N_c(T) \exp\left(-\frac{E_D}{k_B T}\right) \quad (17)$$

This relationship is a useful expression relating the ionization time and the free electron life time. Since the free electron lifetime is arbitrarily chosen, the ionization time can be readily calculated for a given temperature. Using Eqs (12) to (17) the characteristic times can be

calculated for different temperatures. By using the temperature to calculate the Maxwellian time and the recombination time, the relative magnitudes between the characteristic times (τ , τ_i , and τ_M) can be changed such that the three cases mentioned above can be obtained.

Before the characteristic times are actually calculated, a few parameters are needed to use the formulas above. For this reason, an example system is used. As stated earlier, the example system is a BSO crystal subjected to an external electric field. In this numerical model, the field is generated by applying 9 kV across a 0.8 cm long bismuth silicate crystal. The effective mass, m_{eff} , of BSO is fourteen times the mass of an electron, m_e ,⁸ while the permittivity, ϵ , is $50 \epsilon_0$. The free electron mobility, μ , is very dependent on the crystal growth; however, the most notable value for the intrinsic mobility at room temperature is $0.029 \text{ cm}^2 / (\text{volt sec})$.⁹ To complete the initial parameter set before calculating the characteristic times, the energy levels must be known as well as the donor concentration. BSO has energy bandgap, E_{gap} , of 3.25 eV. Within this gap, a realistic donor energy level, E_D , of 0.816 eV from the conduction band is chosen. The typical donor concentration, N_D , is 10^{16} cm^{-3} . This initial parameter set is listed in Table 1 below.

Table 1. Initial parameter set for the crystal.

Parameter Symbol	Value
V	9 kV
d	0.8 cm
m_{eff}	$14 m_e$
ϵ	$50 \times 8.85 \times 10^{-14} \text{ farad/cm}$
μ	$0.029 \text{ cm}^2 / (\text{volt sec})$
E_D	0.816 eV
E_{gap}	3.25 eV
N_D	$1 \times 10^{16} \text{ cm}^{-3}$

With the above initial parameter set and governing equations, the characteristic times for each case are calculated and reported in Table 3. Without redefining the location of the donor energy level to reflect a shallow donor, Case 1 is achieved for the given donor energy level above when the temperature is 800 degrees Kelvin. $T = 800$ K may seem high; however the temperature only reflects the donor energy level being shallow. Case 3 is met for lower temperature such as room temperature, 293 K. It is case 2 that can not be achieved by thermal excitation alone. For this reason, the ionization time for case two is artificially chosen to be four times that of the electron lifetime in case three. This is in effect adding $S \bullet I = 638 \text{ sec}^{-1}$ in Eq (2)'s generation term while maintaining thermal excitation at 293 K. Even though illumination ($S \bullet I$) is initially being used to help generate electrons out of the donor sites, thermal equilibrium still applies since the illumination is “turned off” prior to the application of the external field.

Normalization. In order to facilitate computations, the rate equations given in Chapter II are normalized with respect to the initial transit time $t_0 = d^2/(\mu V)$, the crystal length, the electron concentration when the initial Maxwellian time equals the initial transit time $n_{\text{norm}} = \epsilon V/(\epsilon d^2)$, and the applied electric field, $E_0 = -V/d$.¹ The normalization of a few parameters is given in Table 2. Substituting in the normalization variables into the rate equations (Eqs (3) and (6)) yield the same first rate equation and a slightly modified second rate equation. In Eq (6), the normalized mobility is unity. While the rate equations remain nearly the same, the electric field equation (Eq (7)) is slightly changed. These equations are repeated here for convenience and to clarify that all the parameters from this point are now normalized parameters:

$$\frac{\partial N_D^+}{\partial t} = \frac{(N_D - N_D^+)}{\tau_1} - \frac{n}{\tau} \quad (18)$$

$$\frac{\partial n}{\partial t} = \frac{\partial N_D^+}{\partial t} + \frac{\partial (n E)}{\partial z} \quad (19)$$

$$E(z, t) = E(0, t) + \int_0^1 \rho(z, t) dz \quad (20)$$

where the cathode field is defined as

$$E(0, t) = -1 + \int_0^1 (z - 1) \rho(z, t) dz$$

and the applied voltage is held constant

$$1 = - \int_0^1 E(z) dz$$

Table 2. Conversion to normalized parameters. The primed variables are unnormalized.

Normalized Quantity	Normalization of unnormalized	Normalized Quantity	Normalization of unnormalized
t	t' / t ₀	β	β' t ₀
n	n' / n _{norm}	z	z' / d
γ	γ' t ₀ n _{norm}	E	E / E ₀

Table 3. List of unnormalized and normalized parameter values as well as a description of each.

Parameter Symbol	Unnormalized Value	Normalized Value	Description of Parameter
d	0.8 cm	1	crystal length
E ₀	11250 volt/cm	1	applied electric field
n _{norm}	$3.884 \times 10^{11} \text{ cm}^{-3}$	1	density normalization factor
t ₀	$2.452107 \times 10^{-3} \text{ sec}$	1	transit time
E _D	0.816 eV	0.816 eV	donor energy level
N _D	$1 \times 10^{16} \text{ cm}^{-3}$	25747	donor concentration
N _C (293 K)	$1.269 \times 10^{21} \text{ cm}^{-3}$	3.267×10^9	effective density of states in the conduction band (cases 2 and 3)
N _C (800 K)	$5.726 \times 10^{21} \text{ cm}^{-3}$	1.474×10^{10}	effective density of states in the conduction band (case 1)
n ₀ (293 K)	$2.432 \times 10^{11} \text{ cm}^{-3}$	0.626	number density of free electrons (cases 2 and 3)
n ₀ (800 K)	$7.380 \times 10^{15} \text{ cm}^{-3}$	1.9×10^4	number density of free electrons (case 1)
τ _M (293 K)	0.00392 sec	1.599	Maxwellian relaxation time
τ _M (800 K)	0.000000129 sec	0.0000526	Maxwellian relaxation time
τ _{i1}	0.00458 μsec	1.87×10^{-6}	ionization time (case 1)
τ _{i2}	0.00157 sec	0.64	ionization time (case 2)
τ _{i3}	16.103 sec	6567	ionization time (case 3)
τ ₁	0.0129 sec	5.26	electron lifetime (case 1)
τ ₂	0.000391644 sec	0.1597	electron lifetime (case 2)
τ ₃	0.000391644 sec	0.1597	electron lifetime (case 3)
β ₁	$2.18 \times 10^8 \text{ sec}^{-1}$	5.356×10^5	ionization rate (case 1)
β ₂	636.9 sec^{-1}	1.565	ionization rate (case 2)
β ₃	0.062 sec^{-1}	1.523×10^{-4}	ionization rate (case 3)
γ ₁	$3.187 \times 10^{-10} \text{ cm}^3 \text{ sec}^{-1}$	10	recombination coefficient (case 1)
γ ₂	$1.677 \times 10^{-9} \text{ cm}^3 \text{ sec}^{-1}$	1.597	recombination coefficient (case 2)
γ ₃	$3.187 \times 10^{-10} \text{ cm}^3 \text{ sec}^{-1}$	10	recombination coefficient (case 3)
l ₀ (293 K)	0.1278 cm	0.1597	drift length (cases 2 and 3)
l ₀ (800 K)	$4.2 \times 10^{-6} \text{ cm}$	5.26×10^{-6}	drift length (case 1)
W ₁	0.006 cm	0.0075	steady state depletion layer thickness for case 1
W _{2,3}	1.011 cm	1.264	steady state depletion layer thickness for cases 2 and 3

Results

The results of the numerical calculations are presented in this section. One of the assumptions Furman makes is that the lifetime of the free electrons is constant. The first part

of this section analyzes the electric field dynamics with a constant free electron lifetime in the governing equations (Eqs (18) to (20)); whereas, the second part of this section analyzes the dynamics of the electric field without making such an assumption in the governing equations. In the following analysis, plots of the total electric field as a function of the crystal length is employed to compare Furman's analytical results with the numerical results. As seen in the previous chapter, Furman's equations for Case 1, 2, and 3 predict a movement of the depletion layer thickness toward the anode. Case 3 is the case for which stratification should occur; however, his results did not accurately predict stratification during the observation times that are valid for his solution. While his solutions are invalid for observation times longer than the Maxwellian time, the numerical solutions are valid for all time. For this reason, the numerical results are extended to include times beyond the Maxwellian time to capture the stratification. To facilitate the comparison of the electric fields at different observation times, the following table is created as a guide to the reader. This table allows the reader to compare the observation time in micro seconds to the initial Maxwellian relaxation time and the initial transit time.

Table 4. Comparison of the observation time slices as different ratios.

Value	Value / τ_M	Value / t_0
151.2 μsec	0.039	0.062
302.4 μsec	0.077	0.123
559.5 μsec	0.143	0.228
1512.1 μsec	0.386	0.617
2452.1 μsec	0.626	1.000
3024.3 μsec	0.772	1.233
3916.4 μsec	1.000	1.597
0.025 sec	6.261	10.00
0.049 sec	12.522	20.00
0.074 sec	18.783	30.00
0.123 sec	31.305	50.00
0.245 sec	62.611	100.0
0.368 sec	93.916	150.0

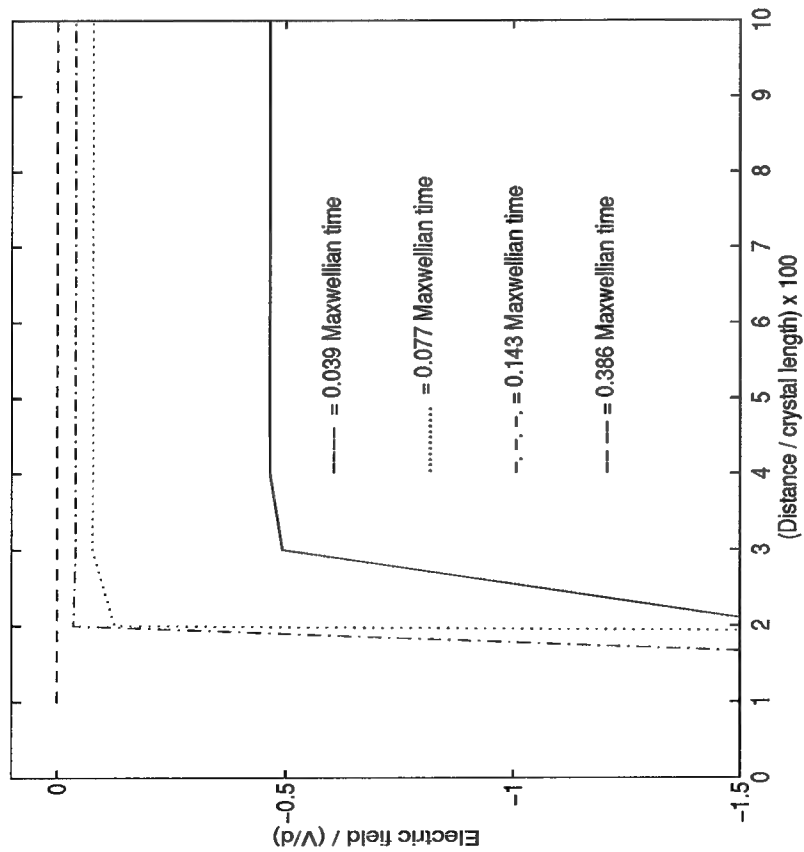
Constant Electron Lifetime Results. Since the electric field dynamics in Case 1 (shallow impurities with $\tau_i \ll \tau$) and Case 2 (deep impurities with $\tau \ll \tau_i \ll \tau_M$) have similar behavior, only Case 2 is presented and analyzed. Case 3 is analyzed in anticipation of observing stratification.

In the analysis, Furman's analytical solutions are compared at identical times with the numerical solutions presented in this research. Since the electric field is spatially and temporally dependent, plots of the field for different times or time slices along the crystal length serve as the method of comparison. In the following paragraphs, Case 2 is analyzed first then Case 3.

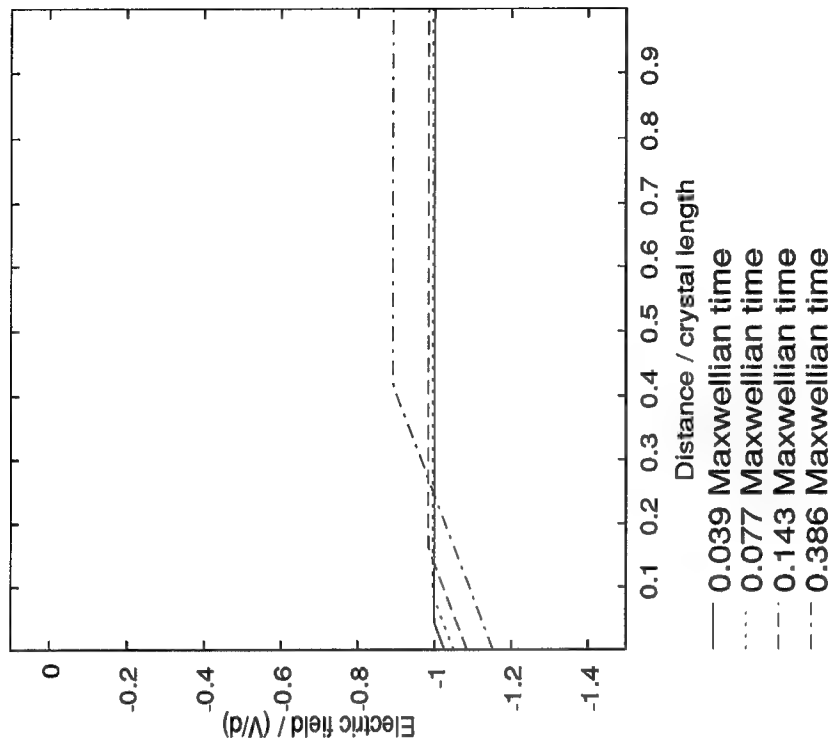
As shown below in Figure 9 for Case 2, a similarity exists between the analytical solution and the numerical solution in terms of the general shape of the electric field. Both solutions predict a linear rise; however, the numerically established value of the electric field rise occurs much closer to the cathode than does the analytic electric field at the same time.

In terms of the velocity of the depletion layer expansion, the analytical solution predicts a higher velocity of expansion. To be specific, at $0.386 \tau_M$, the numerical field reaches steady state around 0.03 d; whereas the analytic field at $0.386 \tau_M$ reaches steady state around 0.9 d. This observation of the depletion region growth could be misinterpreted if no other time slices are observed. A closer observation quickly shows that the analytical depletion region thickness grows away from the cathode; while the numerical depletion region thickness actually narrows or gets closer to the cathode in time. Along with the discrepancy in the depletion region growth along the crystal length, the relative cathode magnitudes are significantly different. As seen in Figure 9, Furman's equations predict the cathode field magnitude to be around 1 to $1.15 E_0$; whereas, the numerical results show the cathode field on the order of $10 E_0$'s. For these reasons alone, one can conclude Furman's analytical expressions are invalid for Case 2.

Where Furman's analytical solutions fail for Case 2, Case 3 analytical solutions and numerical solutions shown in Figure 10 exhibit improved agreement. Both the shapes of the electric fields and the cathode magnitudes of the electric fields at different time slices closely agree in the numerical solution and Furman's analytical solution. As stated earlier, one of the reasons the numerical calculations are performed is to extend the observation time out into the stratification regime. As seen in Figure 11, the oscillations start occurring for observation times around $6 \tau_M$. As the qualitative description predicted in Figure 6, the depletion layer thickness decreases in time and the cathode field increases. As seen in Figure 11, Furman's equations are completely inaccurate in describing stratification. This inaccuracy originates from his equations being invalid for times larger than the Maxwellian time.

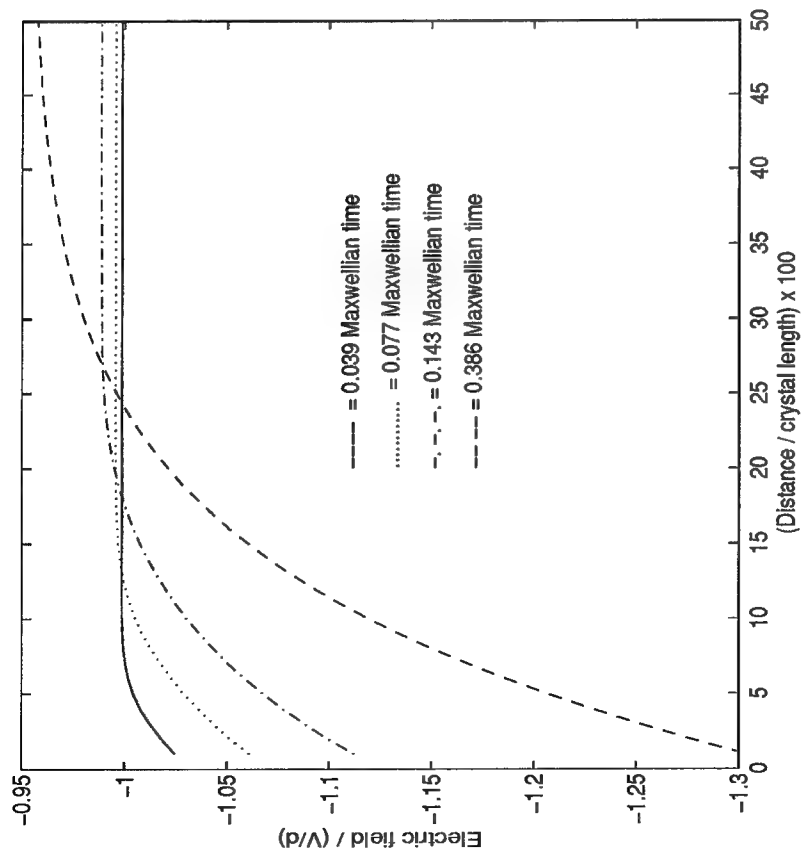


(a)

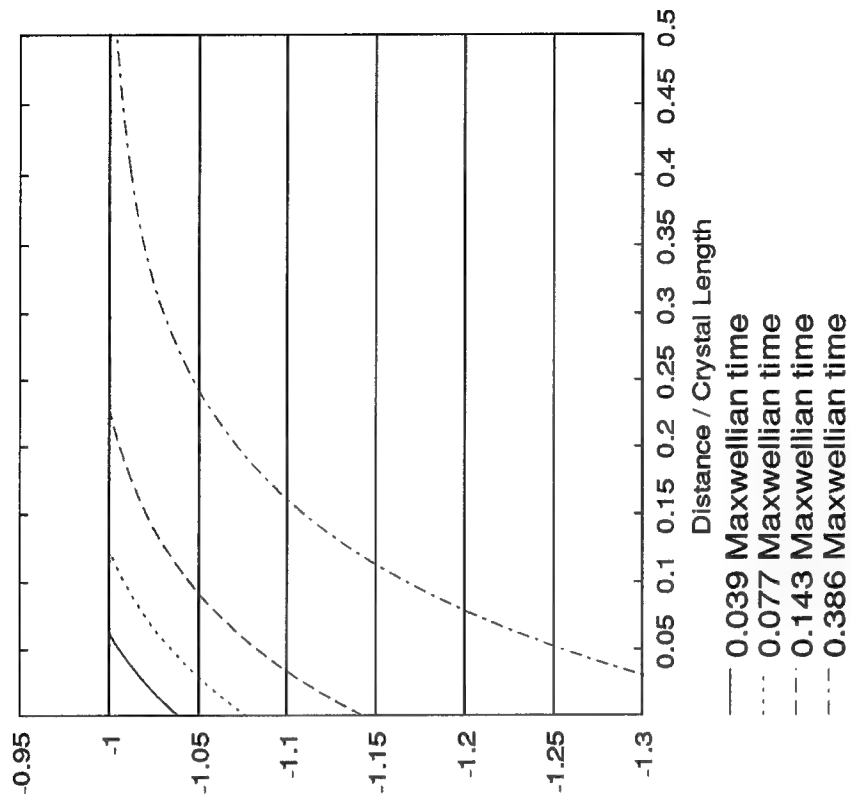


(b)

Figure 9. Case 2 comparison of numerical calculations (a) and analytical calculations (b) of the electric field distribution taken at four specific time slices (see Table 4) and assuming the lifetime of the free electron is constant.

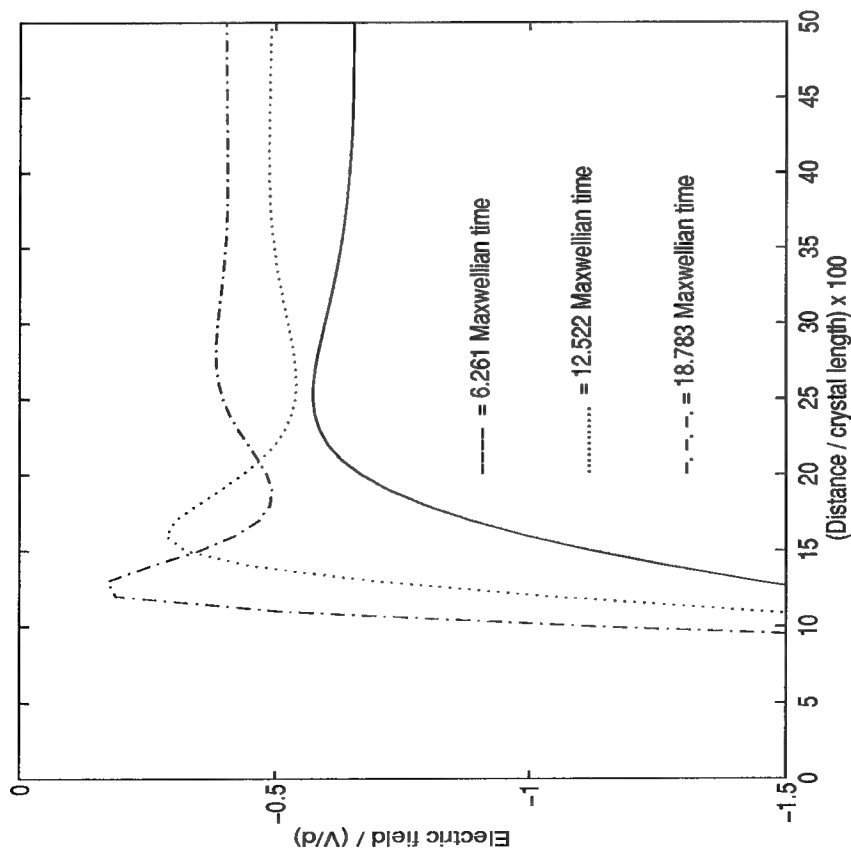


(a)

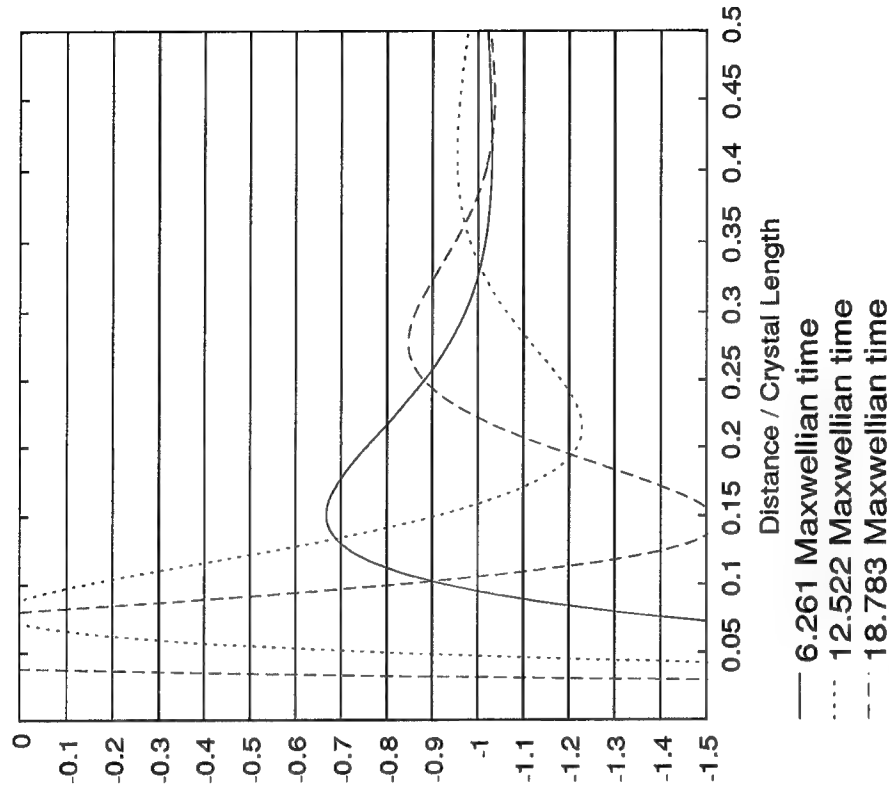


(b)

Figure 10. Case 3 comparison of the numerical calculations (a) and the analytical calculations (b) of the electric field distribution taken at four specific time slices (see Table 4) and assuming the lifetime of the free electron is constant. The depletion layer thickness in both calculations increases in time and no oscillations occur before the Maxwellian time. The movement of the electric fields as well as the cathode field magnitudes are consistent between the numerical results and Furman's analytical results.



(a)



(b)

Figure 11. Extended times larger than the Maxwellian time for Case 3 are used here to compare the numerical calculations and Furman's analytical calculations of the electric field distribution. These plots assume the lifetime of the free electron is constant. The depletion layer size now switches direction and decreases in time. The oscillations that do occur are short lived. Figure (b) is presented here only to emphasize the inaccuracy of Furman's solutions in this time regime.

Explicit Examination of Constant Electron Lifetime Assumption. To try to understand the physical differences between the numerical solutions and Furman's analytical solutions, the lifetime is numerically evaluated and plotted to double check the validity of Furman's assumption of constant free electron lifetime. To do this, Eqs (2) and (6), which include the temporal and spatial dependence of the free electron lifetime, are solved instead of Eqs (18) and (19), which assume a constant free electron lifetime. The results, shown in Figure 12 and Figure 13, show the lifetime is not constant for an observation time larger than about $0.039 \tau_M$. The lifetime is approximately a constant prior to about $0.039 \tau_M$ but quickly varies afterwards due to the changing concentration of ionized donor sites. The $t = 93.916 \tau_M$ curve in Figure 13 suggests the lifetime is approaching a constant value of $0.16 t_0$ at observation times greater than $100 \tau_M$.

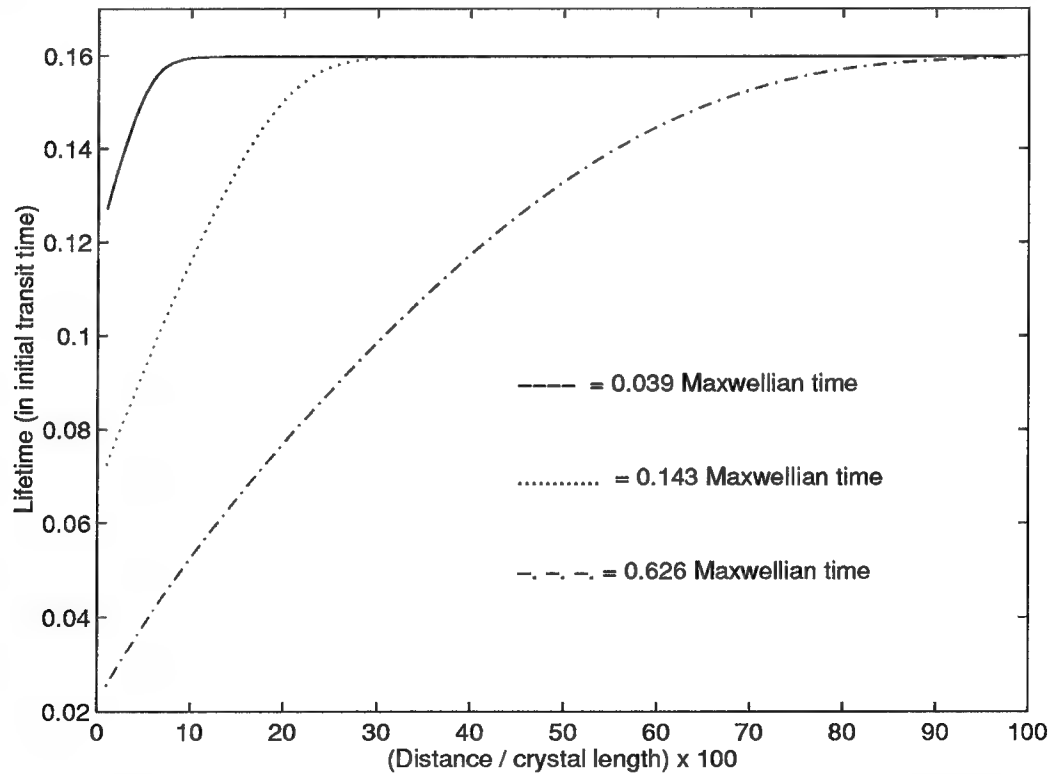


Figure 12. Numerical results depicting a non-constant lifetime of electrons for case three and for specific times slices prior to the transit time (see Table 4).

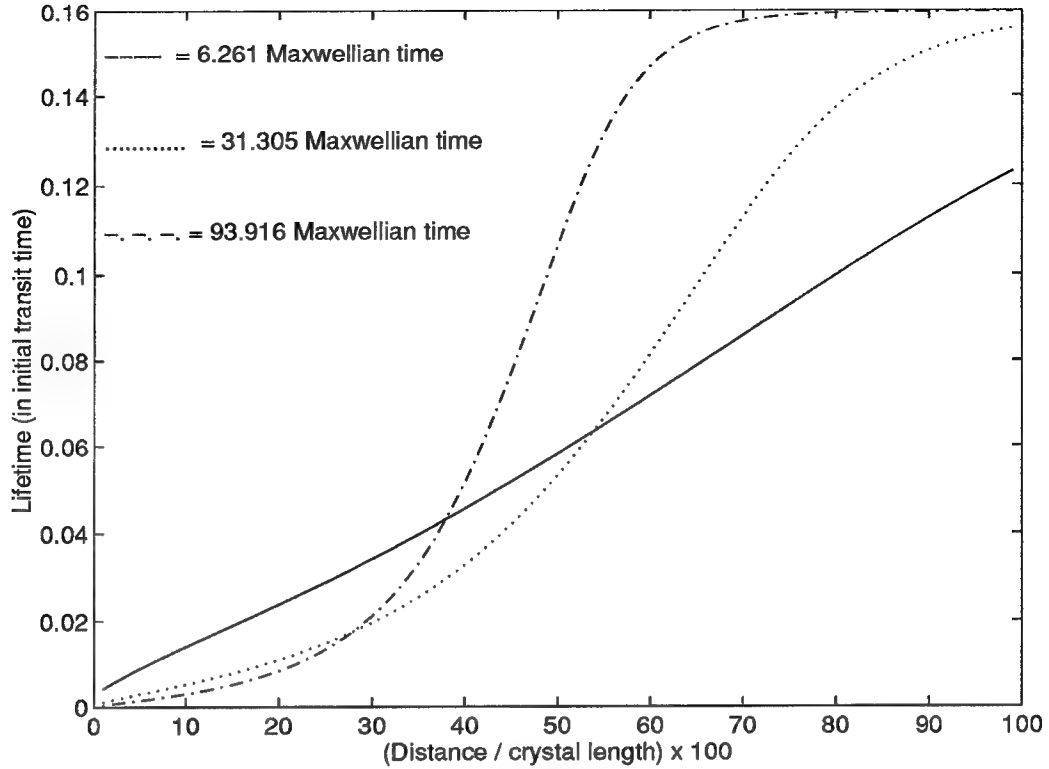


Figure 13. Numerical results depicting a non-constant lifetime of electrons for case three and for specific times slices after the transit time (see Table 4). At later times the system approaches equilibrium and steady state.

Since the lifetime is not constant, Furman's analytical results are proven to be even more inaccurate for the single donor level model. To emphasize, this point, the numerical results for the non-constant lifetime condition are examined using the normalized Eq (2) and Eq (19). Depicted in Figure 14, Case 2 results do not agree with the analytical solution either in depletion layer movement or in field magnitude at the cathode.

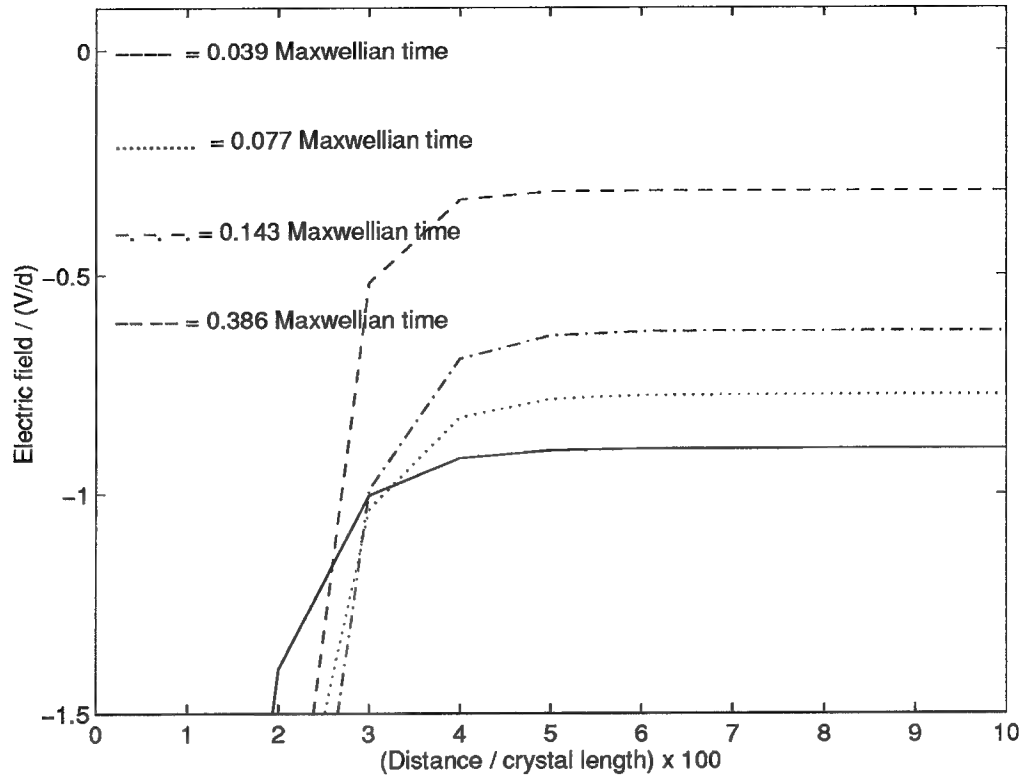


Figure 14. Numerical calculations of the electric field distribution for Case 2 with a non-constant electron lifetime. The electric field does not agree with that predicted by Furman.

As before, the numerical calculations of the electric field distribution in case three do not completely agree with the analytical predictions. The electric field in Figure 15 and Figure 16 demonstrates very similar behavior in depletion layer movement and field magnitude as with the constant τ condition for times less than t_0 (Figure 10), but no oscillations occur even at exaggerated observation times of $376 \tau_M$, which are not shown in these figures.

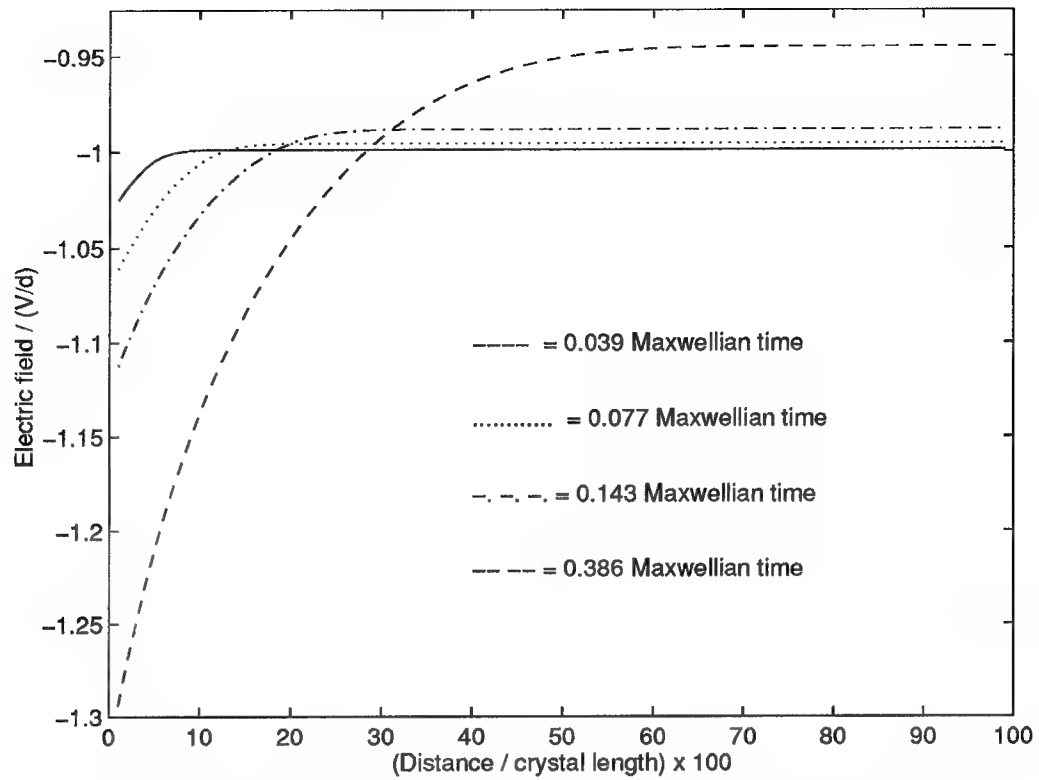


Figure 15. Numerical calculations of the electric field distribution for Case 3 with a non-constant electron lifetime and for times within the transit time. The depletion layer thickness and magnitude increase in time as predicted analytically.

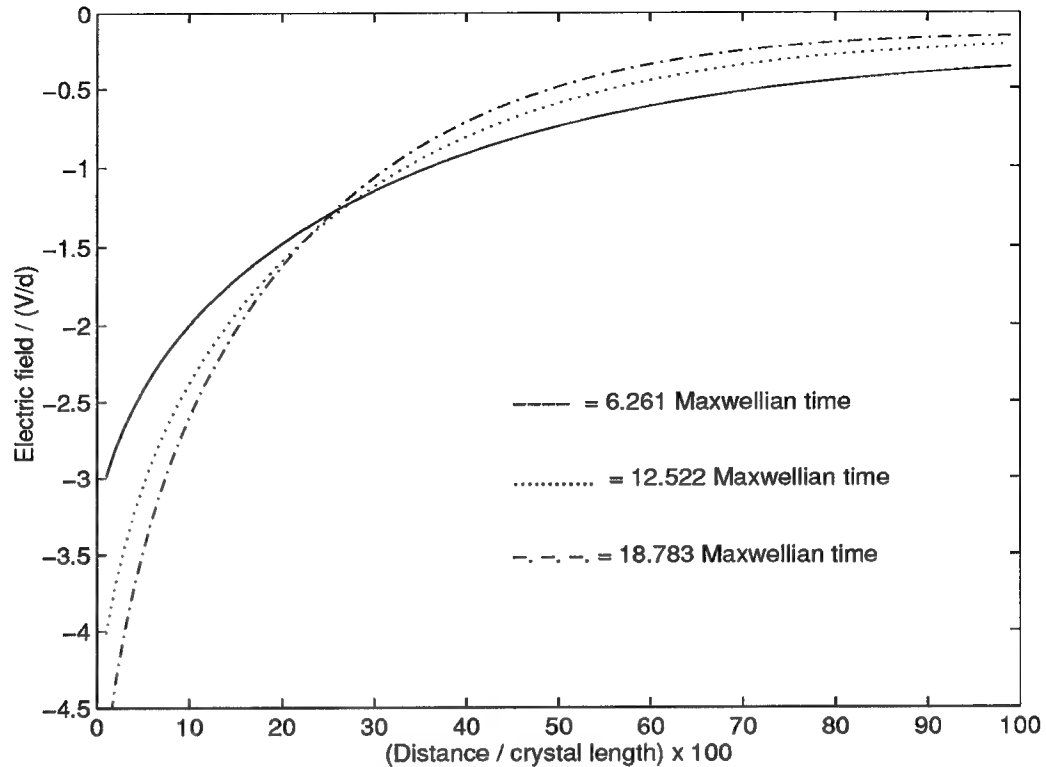


Figure 16. Numerical calculations of the electric field distribution for Case 3 with a non-constant electron lifetime and for times much greater than the transit time. The depletion layer thickness and magnitude increases in time as predicted analytically.

As a result of poor agreement between the numerical predictions and the analytical solutions of the total electric field, the conclusion is that a single donor level does not properly model screening in any of the three cases. To reiterate, the justification for such a statement includes the fact that the free electron concentration is not a constant. Specifically for Case 1 and Case 2, the numerical results and Furman's results predict opposite movement of the depletion layer thickness as well as the electric field magnitude at the cathode. For Case 3, stratification does not occur for all reasonable times. The only area of agreement between the numerical results and Furman's results lies in Case 3 for observation times less than the Maxwellian relaxation time. With the conclusion that a single donor level impurity does not properly model screening in a wide bandgap semiconductor, one is forced to look upon a

possible reason for such a discrepancy between the numerical and analytical results. One may infer that the impurity level is not a donor level but possibility a trap level. For this reason, the set of rate equations is modified to represent a single trap level and the analysis is repeated for a single trap level model in Chapter V.

V. Single Trap Level

Numerical simulation

The previous chapter demonstrated that a single donor level model does not accurately predict the stratification effect; however, Chapter IV suggests that a trap level model may work. For this reason, this chapter addresses a trap level model. As with the donor level model in thermal equilibrium, all the cases discussed in Chapter IV can be achieved in a similar manner for the trap level model in thermal equilibrium. Since the main reason for analyzing the trap level model is to numerically determine if stratification can occur, this chapter focuses on case three, the stratification case. In the following single trap level model analysis, the screening concept is discussed followed by a comparison of numerical results with Furman's results shown earlier.

The process of screening due to trap sites occurs in a slightly different way than with donor sites. In the case of bismuth silicate, the initial concentration of electrons in the traps and the conduction band originally come from uniform photoillumination. It will be assumed that a pulse of photoillumination excites electrons out of a deep donor into the conduction band and then electrons are thermalized between the trap level and the conduction band. At this moment, the uniform photoillumination is turned off and the electrons reach thermal equilibrium between the trap level and the conduction band. Once thermal equilibrium is reached, the modeling time is set to zero: $t = 0$. At $t = 0$, the external electric field is applied and the process of screening begins. Screening involving the trap level is similar to screening with the donor level in terms of electron movement; however, the origin of the positive charge

is governed by the ionized deep donor concentration which is assumed to be uniform and unchanging. Figure 17 gives a band diagram of a simple representation of where the energy levels and charge regions are. As in the donor level model, a net positive region forms near the cathode, while alternate layers of net charge regions form in regions away from the cathode.

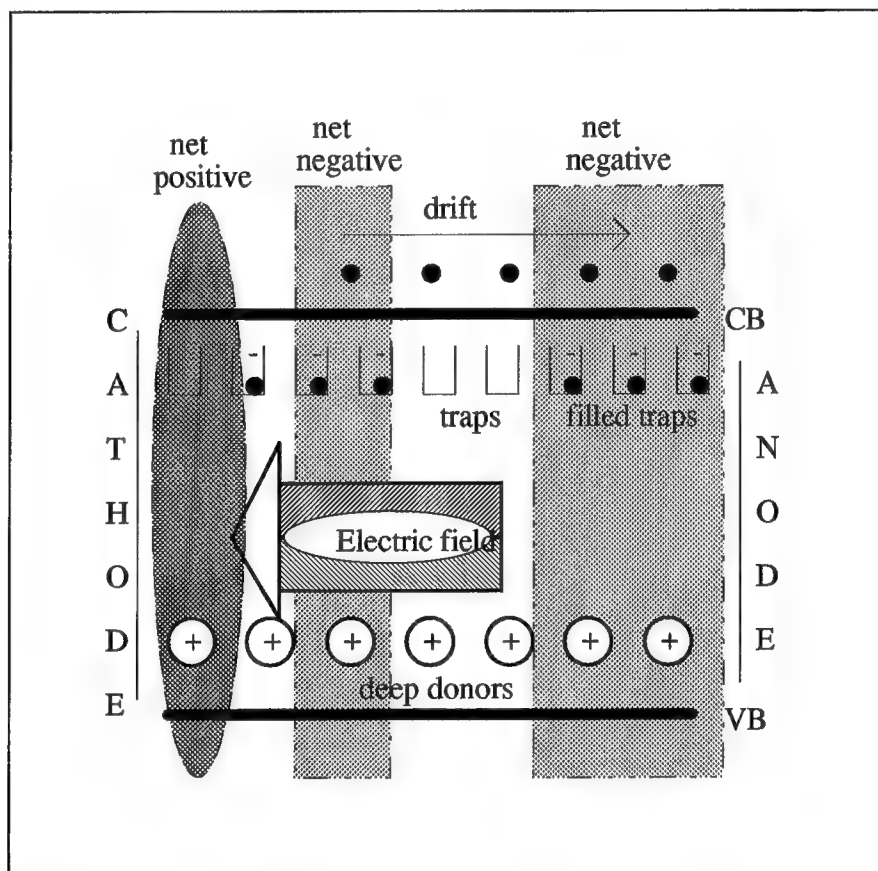


Figure 17. Band diagram showing the ionized trap sites and the free electrons under the influence of an applied voltage.

The rate equations for the trap level model are similar to the single donor level model in that the ionized impurity equation contains a production term and a loss term; however, some differences exist in the ionized trap equations. An ionized trap is a trap site that has

captured a free electron thus taking on a net negative charge. The following rate equation describes the rate of change for the ionized trap:

$$\frac{\partial n_T(z, t)}{\partial t} = -\beta n_T(z, t) + \gamma \cdot n(z, t) (N_T - n_T(z, t)) \quad (21)$$

where $n_T(z, t)$ is the concentration of electrons in the trap, $n(z, t)$ is the concentration of free electrons, β is the ionization rate of trapped electrons to the conduction band, γ is the recombination coefficient for free electrons being captured by the trap, and N_T is the concentration of traps. The recombination process is dependent on the net concentration of unionized traps. For this reason, the second term on the right hand side of Eq (21) contains $n_T(z, t)$ subtracted from N_T . The signs in Eq (21) delineate a loss occurring when a trapped electron is thermally ionized out of the trap and a production occurring when a trap captures a free electron.

As with the donor level, the second rate equation is derived from the continuity equation. Using the same procedure to derive Eq (6), the rate equation describing the rate of change for the free electrons is

$$\frac{\partial n(z, t)}{\partial t} = -\frac{\partial n_T(z, t)}{\partial t} + \mu \frac{\partial [n(z, t) E(z, t)]}{\partial z} \quad (22)$$

where μ is the free electron mobility.

With a proper parameter set, the trap rate equations (Eqs (21) and (22)) can be numerically solved with the same boundary conditions and initial conditions used for the donor level. The parameter set differs from the donor parameter set in the energy level location of the trap, the thermal equilibrium values of initial concentrations, free electron lifetime, and characteristic ionization time. A lower energy level value for the trap site was

chosen to accurately model trap sites within BSO which are typically between 0.2 eV and 0.8 eV.

The trap level is chosen to be 0.45 eV below the conduction band, and for BSO, the photoillumination has a 488nm wavelength to excite electrons from a 2.6 eV deep donor level. Assuming a Maxwellian time of $\tau_M = 0.09$ sec and solving Eq (1) for the initial electron concentration in the conduction band yields $n_0 = 10^{10} \text{ cm}^{-3}$. The initial concentration of electrons in the traps n_{T0} is calculated using the relationship for β / γ ; however, this relationship for traps is slightly different from the donors model (Eq (17) and Appendix C). After rederiving this expression for the trap model, the result is:

$$\beta(T) = 2 \gamma(T) N_c(T) \exp\left(-\frac{E_T}{k_B T}\right) \quad (23)$$

where the factor of 2 originates from the thermal equilibrium expression for the ionized trap concentration. In the derivation, one can assume the ionized trap concentration has the same functional form as an ionized acceptor. With this assumption, Eq (21) can be solved under a steady state condition for β/γ to yield Eq (23). From Eqs (21) and (23), the concentration of electrons in the traps is $n_{T0} = 4.7 \times 10^{13} \text{ cm}^{-3}$. The sum of n_0 and n_{T0} is the total number of electrons generated by uniform photon illumination $n_p = 4.7 \times 10^{13} \text{ cm}^{-3}$. This number is a constant and is reflected in the numerical calculation.

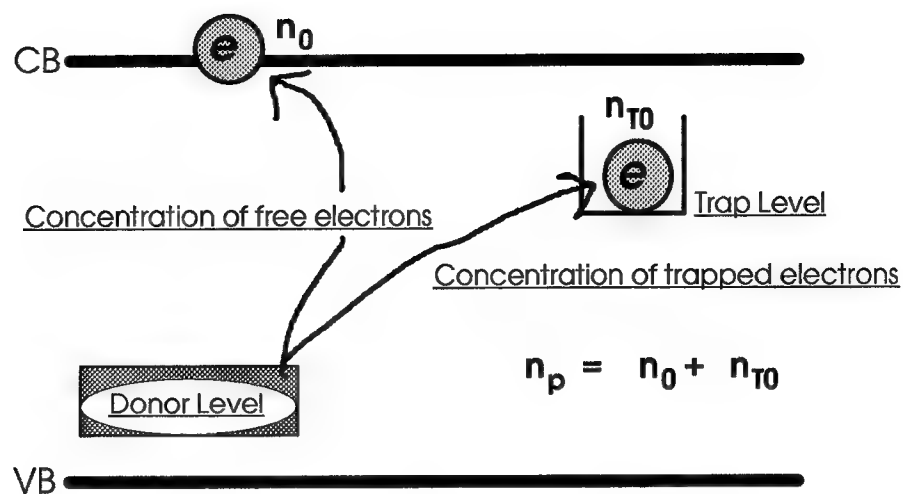


Figure 18. A picture to help explain the different concentrations of electrons involved in the trap model.

As in Chapter IV, the lifetime of the free electrons is arbitrarily chosen. Setting this to be about 100 times smaller than τ_M , $\tau = 0.008$ sec and applying Eq (23), the ionization time becomes $\tau_i = 3.6$ sec. Thus Case 3 is achieved. A long ionization time indicates very little thermal ionization of trapped electrons occurring before electrons are trapped and begin to counter the external electric field. A summary of the characteristic times and concentrations is given in Table 5.

Table 5. Trap level model parameters.

Characteristic Parameter	Characteristic Value
V	9 kV
d	0.8 cm
E _T	0.45 eV
E _{gap}	3.25 eV
N _T	1 x 10 ¹⁶ cm ⁻³
n ₀	10 ¹⁰ cm ⁻³
n _{T0}	4.7 x 10 ¹³ cm ⁻³
n _p	4.7 x 10 ¹³ cm ⁻³
τ _M	0.09 sec
τ	0.008 sec
τ _i	3.6 sec

As a result of going to a trap level model, the recombination coefficient expression changes as well. From Eq (21) this expression becomes:

$$\gamma = \frac{1}{\tau \cdot (N_T - n_T(z, t))} \quad (24)$$

but unless the system is saturated with electrons, N_T is always much greater than n_T(z,t) and the expression simplifies to

$$\gamma = \frac{1}{\tau \cdot N_T} \quad (25)$$

Solving for the lifetime of free electrons τ, yields a constant: the very assumption Furman makes but is invalid for the donor level model.

Results

Using the above relationships for the single trap level model, the internal electric field can be numerically calculated and compared to Furman's analytical results given in Chapters III and IV. As states earlier in this chapter, only Case 3 is analyzed for the single trap level

model. As shown in Figure 19, the outcome does not portray large oscillations in the stratification as expected. The results are very similar in shape to the non-constant lifetime results obtained for the donor model; however, the trap model contains some oscillations at very long time slices, e.g., times that are above 150 transit times. Even so, the oscillations occur much later and with much smaller amplitudes than the ones predicted by Furman.

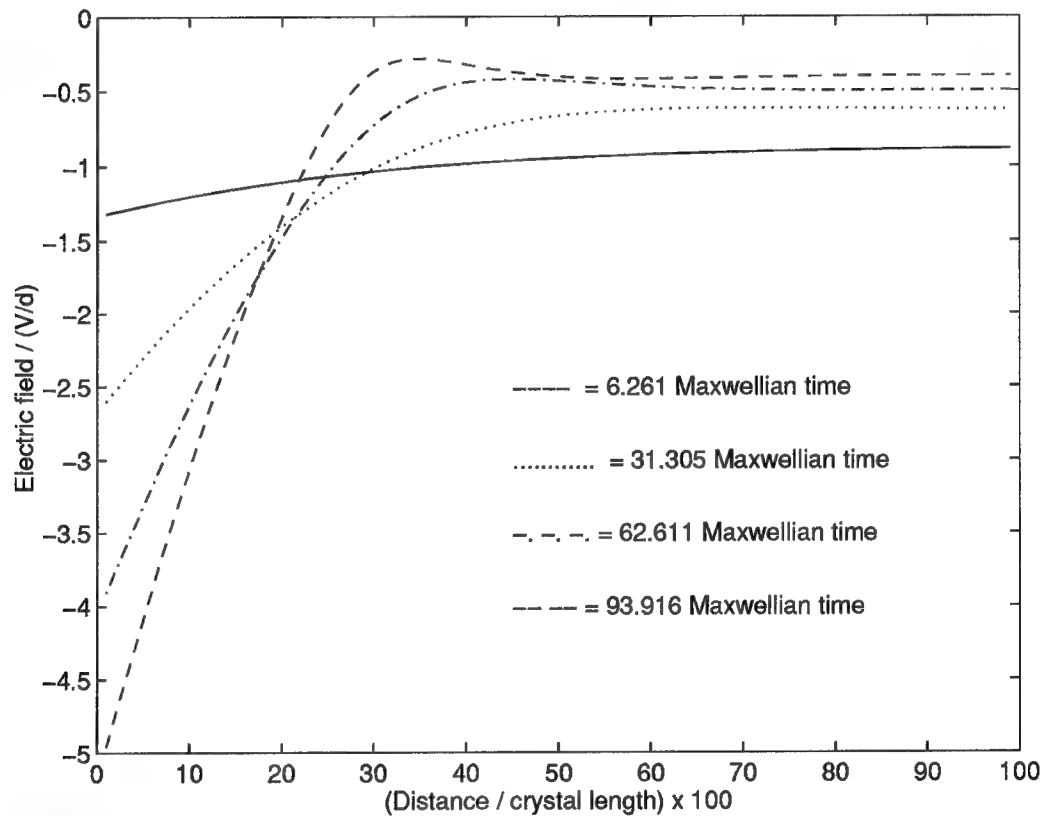


Figure 19. Trap level model of the electric field for Case 3 as a function of the crystal length. Oscillations occur at very long times and with very small amplitude changes.

VI. Conclusions and Recommendations

The attempt to determine if and under what conditions A.S. Furman's analytical solution accurately describes the dynamics of field screening was successful. For a system in thermal equilibrium, Furman's solutions are invalid for shallow impurities ($\tau_i \ll \tau$, Case 1) and for deep impurities ($\tau \ll \tau_i \ll \tau_M$, Case 2), where τ is the free electron lifetime, τ_i is the characteristic ionization time, and τ_M is the Maxwellian relaxation time. In either case, the numerical solutions did not agree with the analytical solutions in both movement of the depletion layer thickness and electric field distribution. For deep impurities ($\tau \ll \tau_M \ll \tau_i$, Case 3), Furman's analytical solutions and the numerical solutions agree for observation times less than the Maxwellian relaxation time τ_M . Because of the assumptions he made in his derivation, Furman's solutions are not applicable for times greater than the Maxwellian time; whereas, the numerical calculations are valid for all time. As seen in Figure 11 and Figure 19, stratification does not occur before τ_M but occurs at very long times, e.g., $t > 6 \tau_M$ for the single donor model and $t > 93 \tau_M$ for the single trap level model. Even at these extended times, the oscillations in the electric field either have small amplitudes or no oscillations at all.

One of the major assumptions Furman makes is the free electron lifetime is constant. As shown in Figure 12 and Figure 13, the free electron lifetime is not a constant for the single donor level model, but from Eq (25) τ is constant for the single trap level model. Thus based upon this one finding, his theory is inaccurate for a single donor level model and is accurate for the single trap level model. As stated above, Furman's analytical solutions are only valid for Case 3 and for times less than the Maxwellian time.

While the model may be accurate for other applications, the conclusion is that Furman's single impurity level analytical model does not accurately predict the oscillatory behavior numerically calculated for bismuth silicate. Along with this discrepancy, neither the results obtained from the single donor model nor from the single trap model agree with behavior experimentally observed for bismuth silicate. For this reason, future work in modeling field dynamics in BSO should consider returning to more than one impurity level models such as the two trap levels model.¹⁰ Future effort should include investigations of the screening behavior of a number of types of photorefractive materials. To accomplish this, other models must be considered. These models may include one or more of the following: two or more trap levels, hole and electron carrier transport, impurity band transport, and injection. Of course, these characteristics can be combinations of each other. Having an understanding of these material models, one can then determine what major influences each of these material models have on the dynamics of screening. The last recommendation for future research is to propose experiments involving screening that can be used to identify material types based upon the models just mentioned.

Appendix A: The PRIZ Device

Photorefractive materials were once regarded as laser damaged materials. The original material, Lithium Niobate, was “damaged” due to a change in refractive index. Later it was discovered that the crystal could return to its original state of refraction by heating it above 200°C.¹¹ Research soon discovered ways to optimize these materials for storage and nonlinear optical applications. One device using photorefractive materials is a spatial light modulator (SLM) called the PRIZ. For the PRIZ, after write light illumination, the readout light intensity is modulated through the transverse electro-optic effect under a longitudinal applied voltage.¹²

The experimental setup of a PRIZ device includes a bismuth silicate crystal sandwiched between transparent electrodes that represent a cathode(-) and an anode(+). An applied voltage, V , to the crystal creates a uniform electric field, $E_0 = -V/d$ through out the crystal. The PRIZ also includes an illuminating beam directed onto the cathode side. For thermal only conditions, no beam is used; whereas, in normal operating conditions, a write-beam and a read-beam are used. The write-beam has a shorter wavelength than the read-beam and is used to create a desired pattern of information within the crystal, e.g., hologram. The read-beam probes the crystal to extract the stored information.

Bismuth silicate (bismuth silicon oxide, $\text{Bi}_{12}\text{SiO}_{20}$) is a wide-bandgap non-centrosymmetric cubic photorefractive crystal used in the PRIZ device. Non-centrosymmetric means that BSO has no center of symmetry. BSO is grown by the standard Czochralski method.¹³ On the average this crystal is yellow-orange in color and is difficult to reproduce

with consistent material properties.¹³ The Russian literature reports that samples taken from the same boule produce significant discrepancies in the properties of the PRIZ spatial light modulators (SLMs).¹⁴ The resulting crystal has a high density of defects and impurity levels of which there is a high density defect that acts much like a deep donor. Located throughout the bandgap of the material are a number of carrier traps. These traps are responsible for collecting mobile carriers and allowing the creation of a refractive index grating by forming nonuniform space charge regions throughout the material.³

While the Czochralski method is the historical growth process, recent work by Rome Laboratory¹⁵ yields high quality BSO crystals produced by hydrothermal techniques--a major step in BSO crystal growth. These clear crystals do not have the deep defects--the very property that allows the PRIZ to behave as a SLM. For this reason, it is necessary to establish the material properties required for such operations in the anticipation of introducing them back into the crystal and creating a controlled nonlinear optical device.

A proper model of the PRIZ device helps to explain the processes that occur during PRIZ operation. Fully understanding the model allows one to have a large insight into understanding what governs the nonlinear optical properties. For the last twenty years, the Russian scientists have been studying the PRIZ both experimentally and theoretically. They have made significant discoveries and breakthroughs in modeling the dynamics that govern the PRIZ operation. The most common and fairly accurate model is the one deep donor and a single trap level. The donor level is considered deep at 2.6 eV below the conduction band in a 3.25 eV bandgap. The trap levels in BSO range from 0.4 to 0.8 eV below the conduction band and are reasonably modeled as one trap level with an energy level within the range given.

Most of the previous AFIT work uses the Russians' two level models. Two levels refer to one donor level and one trap level. A.S. Furman's paper, "Dynamics of screening of an electric field in a semiconductor with a deep impurity level," continues some of the previous work but looks at an analytical solution for a model with only a single impurity level. Furman says the two levels model simplifies to a one level model under certain conditions. Chapters II through V demonstrate that his claim is not as accurate for the stratification effect as he claims.

Appendix B: Derivation of Fermi Energy Level

In order to derive the Fermi energy level, one must apply charge neutrality and solve for the Fermi energy. Under charge neutrality,

$$n_0 + N_d^+ = 0$$

Assuming Maxwell Boltzmann statistics, the equilibrium value of the electron concentration is given by

$$n_0 = N_C \exp\left(\frac{E_F - E_C}{k_B T}\right)$$

where

$$N_C = 2 \left(\frac{2 \pi m_{\text{eff}} k_B T}{h^2} \right)^{3/2}$$

The concentration of ionized donors is given as,

$$N_d^+ = N_d \frac{1}{1 + 2 \exp\left(\frac{E_F - E_D}{k_B T}\right)}$$

where N_d is the donor concentration.

After substituting these two expressions into the charge neutrality condition, one can solve for the Fermi energy level and yield Eq(14). The steps for this derivation are outlined here:

1) Charge neutrality:

$$n_0 + N_d^+ = 0$$

2) Substituting in the thermal equilibrium values for these parameters,

$$N_C \exp\left(\frac{E_F - E_C}{k_B T}\right) + N_d \frac{1}{1 + 2 \exp\left(\frac{E_F - E_D}{k_B T}\right)} = 0$$

3) Multiplying through by the denominator from the second term,

$$N_C \exp\left(\frac{E_F - E_C}{k_B T}\right) + 2 N_C \exp\left(\frac{E_F - E_C}{k_B T}\right) \exp\left(\frac{E_F - E_D}{k_B T}\right) - N_d = 0$$

4) Further simplification,

$$N_C \exp\left(\frac{E_F - E_C}{k_B T}\right) + 2 N_C \exp\left(\frac{2E_F - E_C - E_D}{k_B T}\right) \exp\left(\frac{E_F - E_D}{k_B T}\right) - N_d = 0$$

5) Now make the following substitutions:

$$\beta_C = \exp\left(\frac{-E_C}{k_B T}\right), \quad \beta_D = \exp\left(\frac{-E_D}{k_B T}\right), \quad \alpha = \exp\left(\frac{E_F}{k_B T}\right)$$

6) To yield the following simplified expression:

$$N_C \beta_C \alpha + 2 N_C \beta_C \beta_D \alpha^2 - N_d = 0$$

7) Simplifying into a quadratic expression in terms of α :

$$\alpha^2 + \frac{N_C \beta_C}{2 N_C \beta_C \beta_D} \alpha - \frac{N_d}{2 N_C \beta_C \beta_D} = 0$$

$$\alpha^2 + \frac{1}{2 \beta_D} \alpha - \frac{N_d}{2 N_C \beta_C \beta_D} = 0$$

8) Using the quadratic formula to solve for α yields:

$$\alpha = -\frac{1}{4\beta_D} \pm \sqrt{\frac{1}{16\beta_D^2} + \frac{N_d}{2N_C\beta_C\beta_D}}$$

9) Using the “+” sign, 10) taking the natural logarithm of both sides, and 11) using the law

$$\ln\left(x + \sqrt{x^2 + a^2}\right) = \ln(a) + \sinh^{-1}\left(\frac{x}{a}\right)$$

yields the following expression after doing a little algebra,

$$\ln(\alpha) = \frac{1}{2} \ln\left(\frac{N_d}{2N_C}\right) - \frac{1}{2} \ln(\beta_C\beta_D) + \sinh^{-1}\left(-\sqrt{\frac{N_C}{8N_d}} \sqrt{\frac{\beta_C}{\beta_D}}\right)$$

12) After substituting back in for the expressions for α and β yield Eq(14):

$$E_F(T) = \frac{1}{2} (2E_{\text{gap}} - E_D) + \frac{k_B T}{2} \ln\left(\frac{N_D}{2 N_C(T)}\right) - k_B T \cdot \arcsin\left(\sqrt{\frac{N_C(T)}{8 N_D}} \exp\left(-\frac{E_D}{2 k_B T}\right)\right)$$

where $E_{\text{gap}} = E_C$ ($E_{\text{VALENCE BAND}} = 0$ eV) and $E_D = E_C - E_D$. Notice the E_D in Eq(14) is the energy separation between the conduction band the donor energy level.

*Appendix C: Derivation of β/γ
for the Single Donor Level Model*

Derivation of $\frac{\beta}{\gamma} = N_C \exp\left(-\frac{E_C - E_T}{k \cdot T}\right)$

1) Solve the ionized donor rate equation for steady state:

$$\frac{d}{dt} n_p = \beta \cdot (N_d - n_p) - \gamma \cdot n_p \cdot n \rightarrow 0 = \beta \cdot (N_d - n_p) - \gamma \cdot n_p \cdot n \quad \frac{\beta}{\gamma} = \frac{n \cdot n_p}{N_d - n_p} \quad (1)$$

2) Use known equation for n , n_p , and $N_d - n_p$:

$$n = N_C \exp\left(\frac{E_F - E_C}{k \cdot T}\right) \quad f(E) = \text{Maxwell_Boltzmann_stats} = \frac{1}{1 + 2 \cdot \exp\left(\frac{E_F - E_D}{k \cdot T}\right)} \quad (2)$$

$$n_p = N_d \cdot (1 - f(E)) = N_d \cdot \frac{1}{1 + 2 \cdot \exp\left(\frac{E_F - E_D}{k \cdot T}\right)} \quad N_d - n_p = N_d \cdot \frac{1}{1 + \frac{1}{2} \cdot \exp\left(\frac{E_D - E_F}{k \cdot T}\right)}$$

3) Substitute Eqs.(2) into Eq.(1) and simplify:

$$\frac{\beta}{\gamma} = \frac{n \cdot n_p}{N_d - n_p} = \frac{N_C \exp\left(\frac{E_F - E_C}{k \cdot T}\right) \cdot \left(N_d \cdot \frac{1}{1 + 2 \cdot \exp\left(\frac{E_F - E_D}{k \cdot T}\right)}\right)}{N_d \cdot \frac{1}{1 + \frac{1}{2} \cdot \exp\left(\frac{E_D - E_F}{k \cdot T}\right)}}$$

simplifies to

$$\frac{\beta}{\gamma} = \frac{n \cdot n_p}{N_d - n_p} = \frac{1}{2} N_C \exp \left[\frac{-(-E_F + E_C)}{(k \cdot T)} \right] \cdot \frac{\left[2 + \exp \left[\frac{(-E_F + E_D)}{(k \cdot T)} \right] \right]}{\left[1 + 2 \cdot \exp \left[\frac{-(-E_F + E_D)}{(k \cdot T)} \right] \right]}$$

At this point, one can multiply thru in the numerator and denominator the following:

$$e^{\frac{E_C}{kT}} \cdot e^{\frac{-E_F}{kT}}$$

to yield,

$$\frac{1}{2} \cdot N_C \cdot \frac{2 + e^{\frac{E_D}{kT}} \cdot e^{\frac{-E_F}{kT}}}{e^{\frac{E_C}{kT}} \cdot e^{\frac{-E_F}{kT}} + 2 \cdot e^{\frac{E_C}{kT}} \cdot e^{\frac{-E_D}{kT}}}$$

Now, pull out from the bottom,

$$e^{\frac{E_C - E_D}{kT}}$$

to yield,

$$\frac{1}{2} \cdot N_C \cdot e^{\frac{-E_C - E_D}{kT}} \cdot \frac{2 + e^{\frac{E_D}{kT}} \cdot e^{\frac{-E_F}{kT}}}{e^{\frac{E_C}{kT}} \cdot e^{\frac{-E_F}{kT}} + 2} = \frac{1}{2} \cdot N_C \cdot e^{\frac{-E_C - E_D}{kT}} \cdot \frac{2 + e^{\frac{E_D}{kT}} \cdot e^{\frac{-E_F}{kT}}}{e^{\frac{E_D}{kT}} \cdot e^{\frac{-E_F}{kT}} + 2} = \frac{1}{2} \cdot N_C \cdot e^{\frac{-E_C - E_D}{kT}}$$

THUS,

$$\frac{\beta}{\gamma} = \frac{1}{2} \cdot N_C \cdot e^{\frac{-E_C - E_D}{kT}}$$

Note the extra factor of 1/2 in front.

(3)

=====

References

1. Bryksin, V.V., L.I. Korovin, and Yu. I. Kuz'min, "Role of injection currents in the evolution of a photoinduced charge in photorefractive crystals," *Sov. Phys. Solid State* 29 (5), 757-761 (May 1987).
2. Astratov, V.N., A.V. Il'inskii, and A.S. Furman. "Two Mechanisms of Screening of an Electric Field in High-Resistivity Semiconductors Containing Deep Centers," *Sov. Phys. Solid State* 31 (3), 344 (March 1988).
3. Petrov, M. P., S. I. Stepanov, A.V. Khomenko, Photorefractive Crystals in Coherent Optical Systems, Vol. 59 in Springer Series in Optical Sciences (Springer-Verlag, Berlin, 1991), p. 1.
4. Willardson, Robert K. and Albert C. Beer, Eds., Semiconductors and Semimetals, (Academic Press, New York, 1981), Vol. 15, Chap. 2, p. 64.
5. Astratov, V.N., A.V. Il'inskii, and V.A. Kiselev. "Stratification of the space charge in the case of screening of a field in crystals," *Sov. Phys. Solid State* 26 (9), 1720-1725 (September 1984).
6. Furman, A.S., "Dynamics of screening of an electric field in a semiconductor with a deep impurity level," *Sov. Phys. Semicond.* 22, 1350 (Dec. 1988).
7. McKelvey, John P., Solid State Physics for Engineering and Materials Science, (Krieger Publishing Company, Malabar, Florida, 1993), p. 389.
8. Lauer, R.B., "Electron effective mass and conduction-band effective density of states in $\text{Bi}_{12}\text{SiO}_{20}$," *J. Appl. Phys.* 45 (4), 1794-1797 (April 1974).
9. Hou, S.L., R.B. Lauer, and R.E. Aldrich, "Transport processes of photoinduced carriers in $\text{Bi}_{20}\text{SiO}_{20}$," *J. Appl. Phys.* 44 (6), 2652-2658 (June 1973).
10. Astratov, V.N., A.V. Il'inskii, and A.S. Furman, "Dynamics of electric field screening in photorefractive $\text{Bi}_{12}\text{SiO}_{20}$ crystals," *Sov. Tech. Phys. Lett.* 14 (7), 581-583 (July 1988).
11. Günter, P. "Holography, Coherent Light Amplification and Optical Phase Conjugation with Photorefractive Materials." Physics Reports (Review Section of *Phys. Lett.*) 93, No. 4, 199 (1982). North Holland Publishing Company.
12. Petrov, M. P., S. I. Stepanov, A.V. Khomenko, Photorefractive Crystals in Coherent Optical Systems, Vol. 59 in Springer Series in Optical Sciences (Springer-Verlag, Berlin, 1991), p. 151.

-
13. Petrov, M. P., S. I. Stepanov, A.V. Khomenko, Photorefractive Crystals in Coherent Optical Systems, Vol. 59 in Springer Series in Optical Sciences (Springer-Verlag, Berlin, 1991), p. 233.
 14. Bliznetsov, A.M., V.V. Bryksin, L.I. Korovin, S.V. Miridonov, and A.V. Khomenko. "Injection mechanism of dynamic image selection in PRIZ space-time light modulators," *Sov. Phys. Tech. Phys.* 32(7), 750-754 (July 1987).
 15. Larkin, John, Meckie Harris, and Emery J. Cormier. "Hydrothermal growth of bismuth silicate (BSO)," *Journal of Crystal Growth* 128 (1-4), 871-875 (1 March 1993).

Vita

Second Lieutenant Anthony N. Dills was born February 17, 1971 in Dyersburg, Tennessee. He graduated from Dyersburg High School in Dyersburg, Tennessee in 1989. In June of 1993 he graduated from the United States Air Force Academy with a Bachelor of Science Degree in Physics. He entered the School of Engineering, Air Force Institute of Technology, in June 1993.

Lt. Dills married Deauna Joy of Colorado Springs, Colorado in June of 1993. He has one child who was born in April of 1994.

Permanent Address:

1154 Clanton Road
Dyersburg, Tennessee 38024

REPORT DOCUMENTATION PAGE			Form Approved OMB No. 0704-0188	
Public reporting burden for this collection of information is estimated to average 1 hour per response, including the time for reviewing instructions, searching existing data sources, gathering and maintaining the data needed, and completing and reviewing the collection of information. Send comments regarding this burden estimate or any other aspect of this collection of information, including suggestions for reducing this burden, to Washington Headquarters Services, Directorate for Information Operations and Reports, 1215 Jefferson Davis Highway, Suite 1204, Arlington, VA 22202-4302, and to the Office of Management and Budget, Paperwork Reduction Project (0704-0188), Washington, DC 20503.				
1. AGENCY USE ONLY (Leave blank)		2. REPORT DATE Dec. 1994		3. REPORT TYPE AND DATES COVERED
4. TITLE AND SUBTITLE Model Of A Single Impurity In A Wide Bandgap Semiconductor Describing Electric Field Screening			5. FUNDING NUMBERS	
6. AUTHOR(S) 2Lt. Anthony N. Dills				
7. PERFORMING ORGANIZATION NAME(S) AND ADDRESS(ES) AFIT/ENP			8. PERFORMING ORGANIZATION REPORT NUMBER AFIT/GAP/ENP/94D-3	
9. SPONSORING / MONITORING AGENCY NAME(S) AND ADDRESS(ES)			10. SPONSORING / MONITORING AGENCY REPORT NUMBER	
11. SUPPLEMENTARY NOTES				
12a. DISTRIBUTION / AVAILABILITY STATEMENT This document has been approved for public release and sale; its distribution is unlimited.			12b. DISTRIBUTION CODE	
13. ABSTRACT (Maximum 200 words) A mathematical model of the influence on electric field screening arising from a single impurity in a wide bandgap semiconductor has been numerically investigated and compared with analytically derived solutions. The parameter set chosen to perform the comparison of analytical solution and numerical solution is based upon a bismuth silicate crystal. Both the analytical calculations and the numerical calculations are an attempt to mathematically model the internal electric field within a semiconductor. Two types of impurities were looked at: a single donor level and a single trap impurity level. In general, after an abrupt application of a voltage across the semiconductor, net charge regions begin to redistribute and create internal electric fields that screen the applied field. A trap impurity is found to be more self-consistent with the analytical solutions than a donor impurity; the former satisfying the assumption of a constant free electron lifetime. The analytical solutions are valid for observation times much less than the Maxwellian relaxation time τ_M : $t \ll \tau_M$. The analytical solution properly predicts stratification conditions when the observation time is prior to τ_M ; however, oscillatory behavior, characteristic of stratification, of the internal electric field occurs for times much greater than τ_M . During this regime the analytical solutions are invalid.				
14. SUBJECT TERMS Electric Field Screening, Stratification, Wide Bandgap Semiconductors, Donor Site, Trap Site, Numerical Calculations, Analytical Comparison			15. NUMBER OF PAGES 76	
17. SECURITY CLASSIFICATION OF REPORT Unclassified			18. SECURITY CLASSIFICATION OF THIS PAGE Unclassified	
19. SECURITY CLASSIFICATION OF ABSTRACT Unclassified			20. LIMITATION OF ABSTRACT	